Supporting information for

Electrochemical hydrogenation of nitrogen to ammonia at ambient conditions in a suspended dual-catalyst system

Yue Zhang[a], Wei Sun[a*], Rui-shuang Zhang[a], Yan Feng[a], Bin Dai[a*], Jichang Liu[b]

a: School of Chemistry and Chemical Engineering, Shihezi University, Shihezi, PR China.

b: State Key Laboratory of Chemical Engineering, East China University of Science and Technology, Shanghai, PR China.

***Corresponding author:** Wei Sun, Email: weisun@shzu.edu.cn and 18741354180@163.com.

Bin Dai, Email**:** db_tea@shzu.edu.cn**.**

Contents

Supplementary Table.S1 Various electrochemical systems for ammonia synthesis from N_2 and H_2O at ambient conditions in reported literatures and our work

Electrolyte	Catalysts (Metal wt%)	Current density mA/cm^2	NH_3 yield rate ug/h/g-cat	TOF h^{-1}	FE,%	Detection methods	Ref.
0.5M NaOH	Ru SAs/g-C_3N_4 (0.6wt%)	<0.1	2300	2.28	8.3	Nessler's reagent	[1]
0.1M HCl	Ru/NC (0.1wt%)	~2	3665	21.77	8.5	Indophenol blue method	[2]
0.1M HCl	Ru@ZrO_2/NC (0.1wt%)	~2	1500	8.91	15	Indophenol blue method	[2]
0.05M H_2SO_4	Ru SAs/N-C (0.18wt%)	~0.5	120900	399	29.6	Indophenol blue method	[3]
0.05M H_2SO_4	Ru NPs/N-C (2.64wt%)	~0.5	62500	14.07	14.1	Indophenol blue method	[3]
0.5M K_2SO_4	Ru SAs/Mo_2CTx (1.41wt%)	~0.1	40800	17.19	25.77	Indophenol blue method	[4]
0.1M HCl	RuP_2/rGO (33.54wt%)	~0.2	32300	0.57	13.04	Indophenol blue method	[5]
5mM H_2SO_4	Au_1/C_3N_4 (0.15wt%)	~0.04	1947.8	15.05	11.1	Indophenol blue method	[6]
5mM H_2SO_4	Au NPs/C_3N_4 (3.4wt%)	~0.04	1972	0.67	6	Indophenol blue method	[6]
0.1M Na_2SO_4	FePc/C (0.73wt%)	~0.5	10250	4.63	10.5	Indophenol blue method	[7]
0.1M KOH	Fe-N/C-CNTs (0.5wt%)	~0.8	34830	22.95	9.28	Nessler's reagent	[8]
0.1M KOH	FeSA-N-C (1.09wt%)	<0.05	7480	2.26	56.55	Indophenol blue method	[9]
0.1M HCl	Au/CeOx–RGO (1.31wt%)	<0.1	8300	7.34	10.1	Indophenol blue method	[10]
0.1M HCl	Au/TiO_2 (1.542wt%)	~0.4	21400	16.08	8.11	Indophenol blue method	[11]
0.5M Li_2SO_4	PEBCD/C (----)	~1	2010	----	1.71	Nessler's reagent	[12]
0.05M H_2SO_4	NPC (----)	~4.5	23800	----	1.42	Nessler's reagent	[13]
0.5mM SiW_{12}	Ru/TiO_2 (0.28wt%)	0.1 1 10 100	192.2 265.2 2446.1 16691.3	0.41 0.56 5.19 35.42	42.9 5.92 5.46 3.73	Nessler's reagent	This work

FE is the faradaic efficient.

Supplementary Table.S2 Various electrochemical systems for ammonia synthesis under ambient pressure and different temperatures in reported literatures and our work

T, ℃	Electrolyte	Cathode	Reactants	Current density mA/cm^2	NH_3 yield rate $ug/h/cm^2$	FE,%	Detection methods	Ref.
550	$BaCe_{0.2}Zr_{0.7}Y_{0.1}O_{2.9}$	Ni-BZCY72	H_2-N_2	12.5	175.03	6.2	Cavity Ringdown Spectroscopy	[14]
550	$La_{0.9}Sr_{0.1}Ga_{0.8}Mg_{0.2}O_{3-\alpha}$	Ag-Pd	H_2-N_2	2.1	145.04	70	Nessler's reagent	[15]
550	$BaZr_{0.8}Y_{0.2}O_{3-\delta}$	Ag	H_2O-N_2	4.5	3.00	0.46	Indophenol blue method	[16]
550	$BaZr_{0.8}Y_{0.2}O_{3-\delta}$	LCSF	H_2O-N_2	5.5	5.20	0.33	Indophenol blue method	[16]
500	$BaCe_{0.9}Y_{0.1}O_{3-\delta}$	Ru/LSTR	H_2-N_2	0.45	0.31	2	Liquid chromatography	[17]
500	$BaCe_{0.9}Y_{0.1}O_{3-\delta}$	Ag-Pd	H_2-N_2	0.8	1.84	<1	Liquid chromatography	[17]
500	$BaCe_{0.85}Y_{0.15}O_{3-\alpha}$	Ag-Pd	H_2-N_2	1.0	128.52	60	Spectro-photometry	[18]
450	SDC-ternary carbonate	(LSFCu) -SDC	H_2-N_2	55	329.87	7.5	Nessler's reagent	[19]
450	$LiAlO_2$-$(Li/Na/K)_2CO_3$	Co_3Mo_3N-Ag	H_2-N_2	3.21	20.01	3.83	Nessler's reagent	[20]
400	Carbonate-$LiAlO_2$	$CoFe_2O_4$-Ag	H_2-N_2	3.0	14.20	2.30	Nessler's reagent	[21]
400	$Ce_{0.8}Gd_{0.18}Ca_{0.02}O_{2-\delta}$	(LSFCu)-CGDC	H_2O -N_2/Air	14.5	3.06	0.39	Ammonia ISE analysis	[22]
300	LiCl, KCl, CsCl (0.5% Li_3N)	Porous Ni Plate	H_2O-N_2	25	354.96	80	IR spectroscopy	[23]
300	LiCl, KCl, CsCl (0.5% Li_3N)	Porous Ni Plate	H_2O-N_2	23	1224.0	23	IR spectroscopy	[24]
200	NaOH/KOH Nano-Fe_2O_3	Ni	H_2O-N_2	200	612.0	35	UV/vis, ISE, Test strips	[25]
200	$Na_{0.5}K_{0.5}OH$ Nano-Fe_2O_3	Monel (Ni-Cu)	H_2O-N_2	20	991.44	76	UV/vis, ISE, Test strips	[26]
90	Nafion	Ru	H_2O-N_2	2.6	1.30	0.92	Ion Chromatography	[27]
80	Nafion	Pt	H_2O -Air	10	57.34	0.83	Nessler's reagent	[28]
Ambient	0.5mM SiW_{12}	Graphite rod (with suspended Ru/TiO_2)	H_2O-N_2	0.1 1 10 100	192.2 265.2 2446.1 16691.3	42.9 5.92 5.46 3.73	Nessler's Reagent	This work

Supplementary Table.S3 Comparison of ammonia NH_3 generation rate in literatures (hydrogenation of nitrogen N_2 with hydrogen H_2: $N_2+ H_2 \rightleftharpoons NH_3$) with this study.

No.	Catalysts	Metal (wt%)	Tem./Pre. (H_2/N_2)	[a]NH_3 yield umol/g/h	Ea kJ/mol	[b]NH_3 yield(25 ℃) umol/g/h	[c]TOF(25 ℃) s^{-1}	Ref
1	Ru/C12A7:e^-	1.2(Ru)	360 ℃, 1atm (3:1)	1820	49	0.052	1.21×10^{-7}	[29]
2	Ru/C12A7:O^{2-}	1.2(Ru)	360 ℃, 1atm (3:1)	250	104	5.62×10^{-8}	1.31×10^{-13}	[29]
3	Ru/CaO•Al_2O_3	1.2(Ru)	360 ℃, 1atm (3:1)	150	118	1.70×10^{-9}	3.97×10^{-15}	[29]
4	Ru-Cs/MgO	6(Ru)	360 ℃, 1atm (3:1)	1720	99	1.13×10^{-6}	5.26×10^{-13}	[29]
5	Ru/C12A7:H^-	1(Ru)	360 ℃, 1atm (3:1)	90	154	4.66×10^{-13}	1.31×10^{-18}	[29]
6	Ru/γ-Al_2O_3	6(Ru)	400 ℃, 1atm (3:1)	51	64.4	2.61×10^{-5}	1.22×10^{-11}	[30]
7	Ru/CaO	1.5(Ru)	400 ℃, 1atm (3:1)	158	120.1	2.94×10^{-10}	5.50×10^{-16}	[30]
8	Ba-Ru/AC	1(Ru)	400 ℃, 1atm (3:1)	148	88.8	3.14×10^{-7}	8.81×10^{-13}	[30]
9	Ba-Ru/AC	9.1(Ru)	400 ℃, 1atm (3:1)	2228	72.5	1.85×10^{-4}	5.70×10^{-11}	[30]
10	Cs-Ru/MgO	1(Ru)	400 ℃, 1atm (3:1)	2264	85.8	9.43×10^{-6}	2.65×10^{-11}	[30]
11	Cs-Ru/MgO	6(Ru)	400 ℃, 1atm (3:1)	3353	73	2.48×10^{-4}	1.16×10^{-10}	[30]
12	Ru/C12A7:O^{2-}	1.2(Ru)	400 ℃, 1atm (3:1)	546	104.6	3.32×10^{-8}	7.75×10^{-14}	[30]
13	Ru/C12A7:e-	0.1(Ru)	400 ℃, 1atm (3:1)	715	53.6	0.0042	1.17×10^{-7}	[30]
14	Ru/C12A7:e-	0.3(Ru)	400 ℃, 1atm (3:1)	1027	40	0.13	1.19×10^{-6}	[30]
15	Ru/C12A7:e-	1.2(Ru)	400 ℃, 1atm (3:1)	2757	49.1	0.044	1.03×10^{-7}	[30]
16	Ru/C12A7:e-	4(Ru)	400 ℃, 1atm (3:1)	2122	56	0.0072	5.05×10^{-9}	[30]
17	Ru/C12A7:e^-(HT)	2(Ru)	340 ℃, 1atm (3:1)	2290	53	0.039	5.41×10^{-8}	[31]
18	Ru/C12A7:e^-(SP)	2(Ru)	340 ℃, 1atm (3:1)	1180	49	0.046	6.38×10^{-8}	[31]
19	Ru/Ca_2N:e^-	1.8(Ru)	300 ℃, 1atm (3:1)	1674	60	0.015	2.34×10^{-8}	[32]

20	Ru/CaNH	1.8(Ru)	300 ℃, 1atm (3:1)	53	110	2.95×10^{-8}	4.60×10^{-14}	[32]
21	Ru/C12A7:e^-	1.8(Ru)	300 ℃, 1atm (3:1)	745	51	0.038	5.95×10^{-8}	[32]
22	Ru/CaH_2	2(Ru)	300 ℃, 1atm (3:1)	2549	71	0.0027	3.80×10^{-9}	[32]
23	Ru–Cs/MgO	2(Ru)	300 ℃, 1atm (3:1)	697	120	5.60×10^{-8}	7.85×10^{-14}	[32]
24	Ru/BaO-CaH_2	10(Ru)	340 ℃, 1atm (3:1)	10500	41	2.13	5.97×10^{-7}	[33]
25	Ru/CaH_2	10(Ru)	340 ℃, 1atm (3:1)	7400	68	0.0055	1.56×10^{-9}	[33]
26	Ru/Ba-$Ca(NH_2)_2$	10(Ru)	340 ℃, 1atm (3:1)	12400	44	1.35	3.79×10^{-7}	[33]
27	Ru/Y_5Si_3	2(Ru)	400 ℃, 1atm (3:1)	800	48	0.016	2.30×10^{-8}	[34]
28	Ru/Y_5Si_3	5(Ru)	400 ℃, 1atm (3:1)	1400	50	0.018	1.03×10^{-8}	[34]
29	Ru/Y_5Si_3	7.8(Ru)	400 ℃, 1atm (3:1)	1900	52	0.016	5.70×10^{-9}	[34]
30	Ru/LaScSi	1.8(Ru)	400 ℃, 1atm (3:1)	2800	52	0.023	3.64×10^{-8}	[35]
31	Ru/LaScSi	4.4(Ru)	400 ℃, 1atm (3:1)	3000	52	0.025	1.59×10^{-8}	[35]
32	Ru/LaScSi	8.3(Ru)	400 ℃, 1atm (3:1)	3400	49	0.056	1.88×10^{-8}	[35]
33	Co/C12A7:e^-	2.6(Co)	400 ℃, 1atm (3:1)	1764	49.5	0.026	1.63×10^{-8}	[36]
34	Co/C12A7:O_2	2.9(Co)	400 ℃, 1atm (3:1)	48	112.7	4.72×10^{-10}	2.66×10^{-16}	[36]
35	Ba−Co/AC	10(Co)	400 ℃, 1atm (3:1)	104	98.3	2.60×10^{-8}	4.27×10^{-15}	[36]
36	Cs−Co/MgO	6(Co)	400 ℃, 1atm (3:1)	149	108.9	3.44×10^{-9}	9.40×10^{-16}	[36]
37	Co_3Mo_3N	---	400 ℃, 1atm (3:1)	652	56	0.0022	---	[37]
38	Ni-Mo-N	---	400 ℃, 1atm (3:1)	275	53	0.0018	---	[37]
39	Fe-Mo-N	---	400 ℃, 1atm (3:1)	143	47	0.0037	---	[37]
40	Mo_2N	---	400 ℃, 1atm (3:1)	68	52	5.67×10^{-4}	---	[37]

41	Ru/CaFH	12(Ru)	50 ℃, 1atm (3:1)	50	20	26.77	6.26×10^{-6}	[38]
42	Ru/MgX	2.21(Ru)	400 ℃, 20atm (3:1)	2804	147	1.23×10^{-11}	1.56×10^{-17}	[39]
43	Ru/CsX	1.82(Ru)	400 ℃, 20atm (3:1)	993	82	9.72×10^{-6}	1.50×10^{-11}	[39]
44	Ru/KX-1	2.16(Ru)	400 ℃, 20atm (3:1)	993	124	7.68×10^{-10}	9.98×10^{-16}	[39]
45	Ru/BaX-1	2.02(Ru)	400 ℃, 20atm (3:1)	1980	173	2.51×10^{-14}	3.48×10^{-20}	[39]
46	Co-Ba/C	---	400 ℃, 10atm (3:1)	22320	102	2.43×10^{-6}	---	[40]
47	Co-Sr/C	---	400 ℃, 10atm (3:1)	5040	110	9.09×10^{-8}	---	[40]
48	Fe(KM1)	---	400 ℃, 10atm (3:1)	37800	70	0.0055	---	[40]
49	Co/C	---	400 ℃, 10atm (3:1)	79.2	149	2.22×10^{-13}	---	[40]
50	Fe/C	---	400 ℃, 10atm (3:1)	7560	143	8.15×10^{-11}	---	[40]
51	Fe-LiH	---	300 ℃, 10atm (3:1)	4500	46.5	0.55	---	[41]
52	Mn-LiH	---	300 ℃, 10atm (3:1)	3000	50.6	0.17	---	[41]
53	Co-LiH	---	300 ℃, 10atm (3:1)	4800	52.1	0.20	---	[41]
54	Cr-LiH	---	300 ℃, 10atm (3:1)	3500	63.6	0.016	---	[41]
55	SiW_{12}-Ru/TiO_2	0.28(Ru)	25 ℃, 1atm (---)	981.8	---	---	9.84×10^{-3}	This work

a: Ammonia yield was experimentally determined at the given temperature and pressure (H_2/N_2), where H_2/N_2 is the volume ratio of hydrogen H_2 to nitrogen N_2 in feedstock.

b: Ammonia yield at 25 ℃ was extrapolated from the experimentally determined ammonia yield and activation energy E_a.

c: TOF was calculated from the ammonia yield divided by the number of metal atoms deposited on the catalysts.

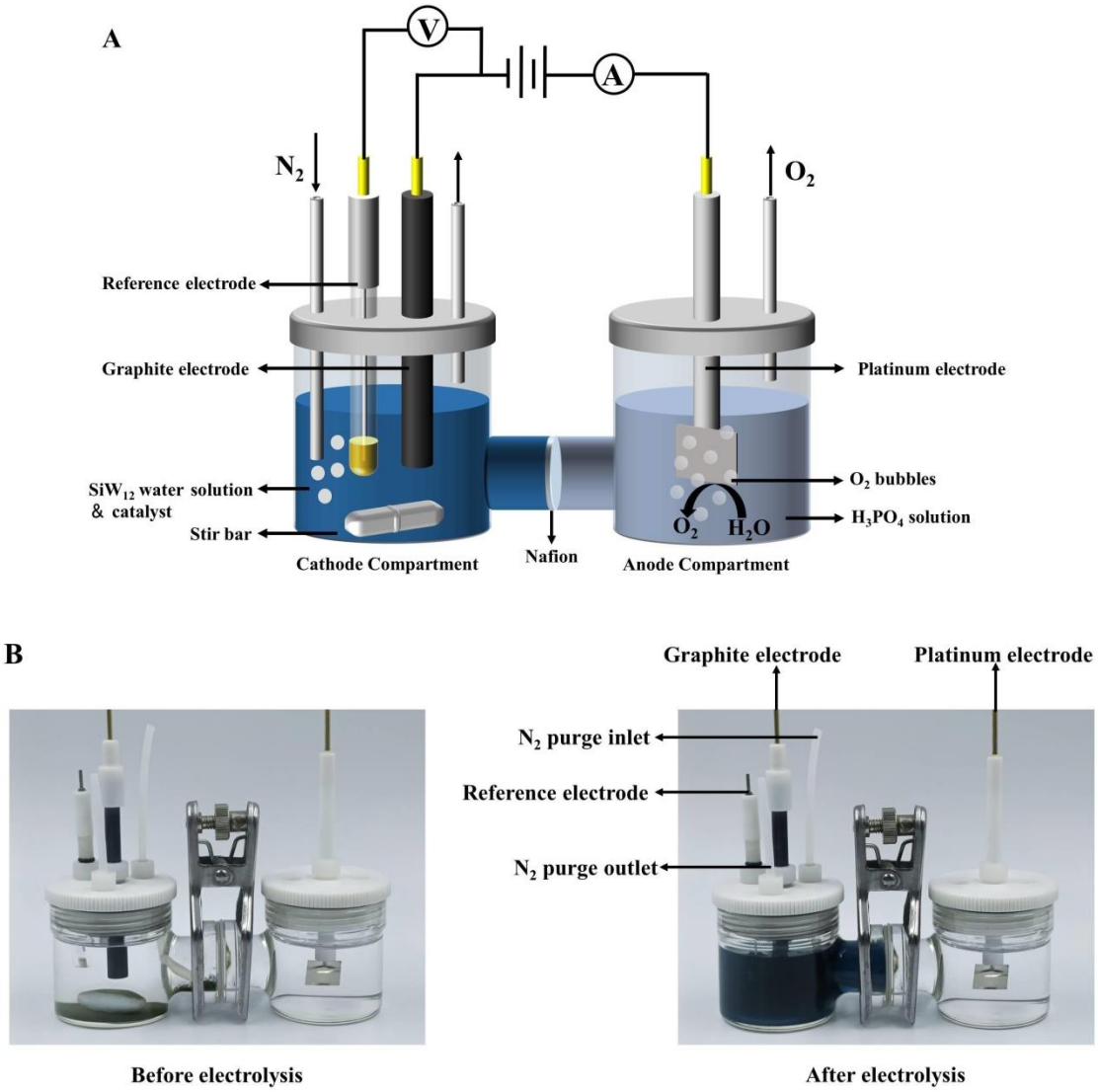

Supplementary Fig.S1 (A) Schematic illustration for three-electrode system of SiW_{12} mediated electro-hydrogenation. (B) Photograph of the experimental setup. The SiW_{12} reaction solution in cathode compartment is colorless before electro-reduction, and the color turns to dark blue after electrolysis.

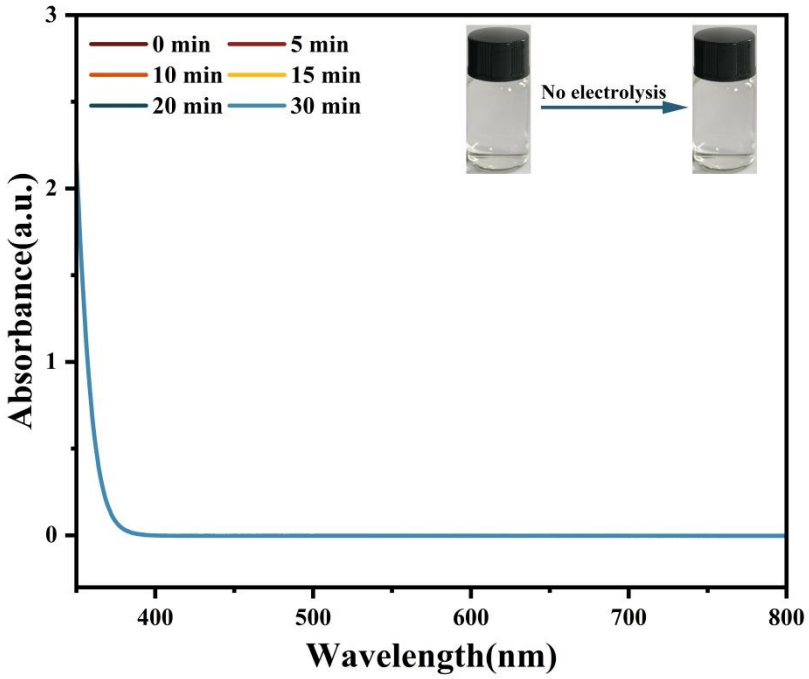

Supplementary Fig.S2 Chronologically recorded UV-Vis spectra of SiW_{12} solution (0.5g SiW_{12}, 35mL H_2O) without electrolysis. The inset photographs demonstrate the SiW_{12} solution having no color change without electrolysis.

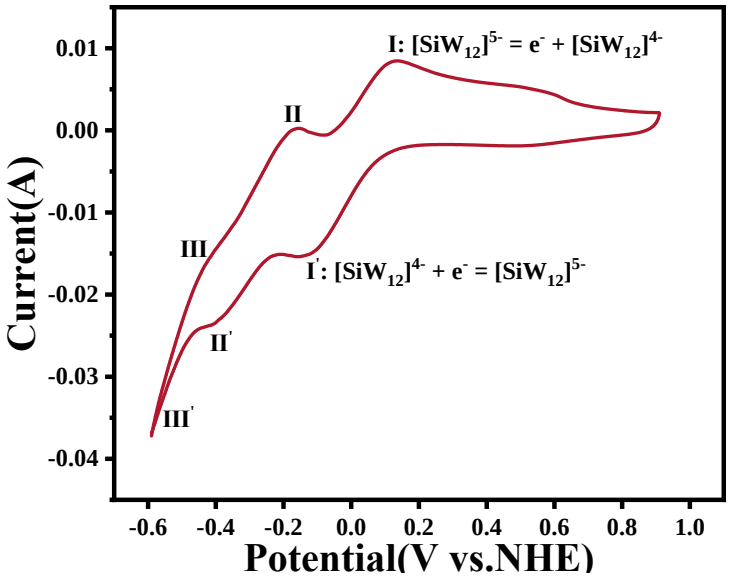

Supplementary Fig.S3 Cyclic voltammogram of SiW_{12} solution (scanning conditions: working electrode: Pt sheet; reference electrode: Ag/AgCl; SiW_{12} concentration: 0.05mol/L; temperature: 20^{o}C; scanning rate: 10mV/s). The curve of SiW_{12} includes three redox waves: the waves centered at around +0.10 V (I), -0.20V (II) and -0.40V (III). The first two waves are ascribed to two one-electron reduction processes and the third wave corresponds to a proton associated two-electron reduction[42].

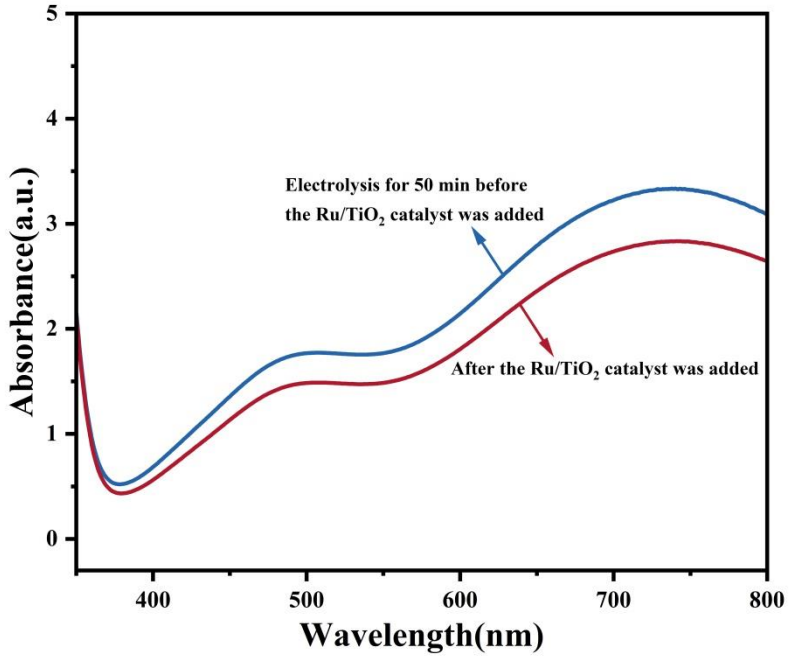

Supplementary Fig.S4 UV-Vis spectra of SiW_{12} solutions before and after adding 0.05g Ru/TiO_2 catalyst particles under a constant electrolysis current density of 100 mA/cm^2. The UV-Vis spectra were measured by taking out 5mL sample from SiW_{12} solutions (0.5g SiW_{12}, 35mL H_2O) which were electrolyzed 50min.

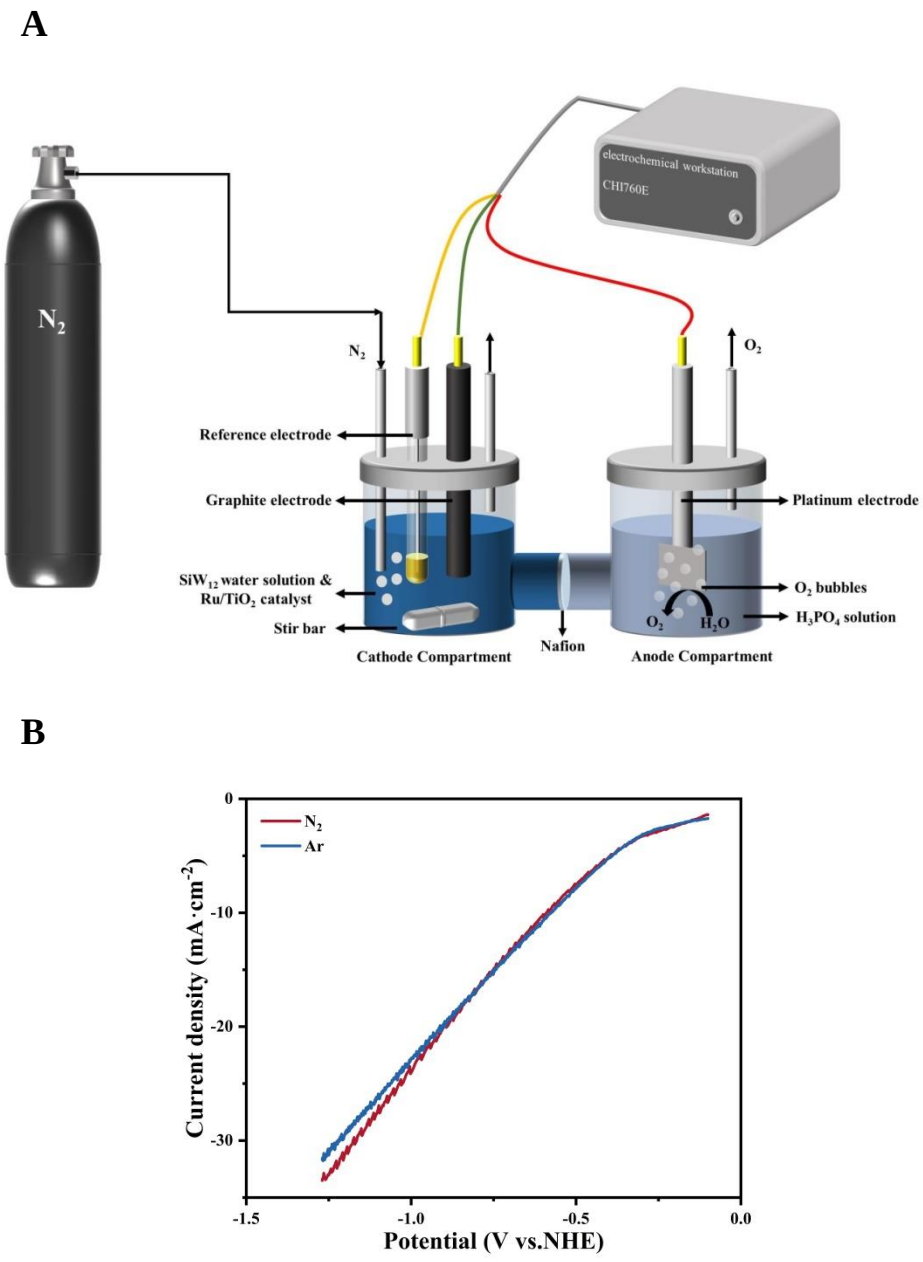

Supplementary Fig.S5 (A) Illustration of three-electrode electrolysis experimental setup for electrochemical hydrogenation of nitrogen into ammonia. (B) LSV curves in 5mM SiW_{12} solution suspended with 0.05g Ru/TiO_2 under N_2 and Ar atmospheres. The scan rate is 10mV/s. It can be found that the current density of solution under N_2 atmospheres become larger and larger than that under Ar atmospheres as the reaction proceeds. This could be ascribed to the ammonium ions produced when N_2 gas is bubbled into solution.

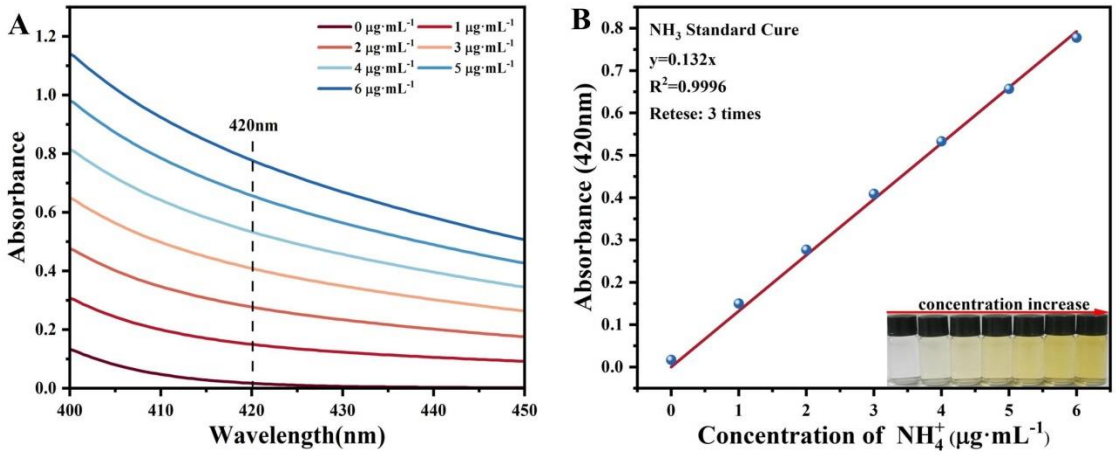

Supplementary Fig.S6 (A) The UV-Vis absorbance of NH_4Cl aqueous solutions with known NH_4Cl concentrations. (B) Standard curve of the absorbance at 420nm of NH_4Cl aqueous solutions with different NH_4Cl concentrations. The absorbance at 420nm shows a strong linear correlation with the NH_4Cl concentrations, indicating the relationship is in accordance with the Beer-Lambert Law. The Standard curve was measured 3 times.

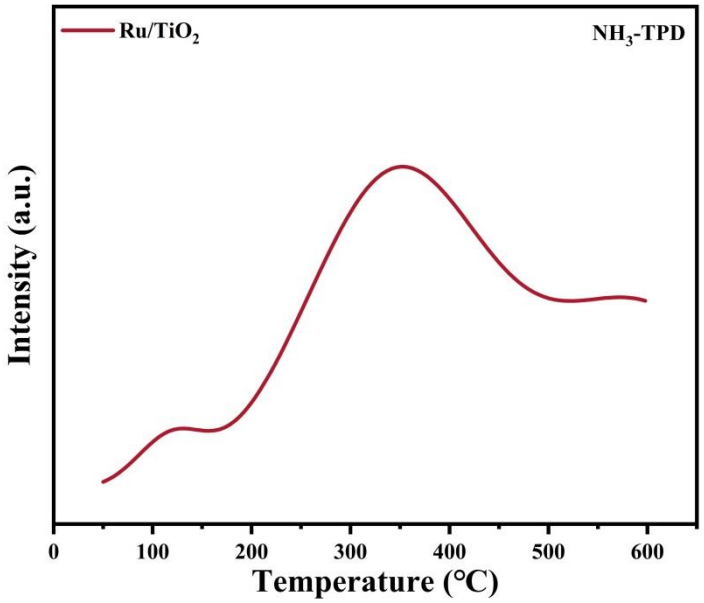

Supplementary Fig.S7 TPD spectra of NH_3 from Ru/TiO_2 catalyst after exposure to NH_3 at 50^{o}C for 1h. Ru/TiO_2 catalyst displays three TPD peaks, one centered at ~118 ^{o}C, the other two centered at ~346.5 ^{o}C and ~593 ^{o}C respectively. Moreover, relative low NH_3 response below 100 ^{o}C was observed, suggesting the adsorption of NH_3 on Ru/TiO_2 is very strong and most of NH_3 generated on Ru/TiO_2 are difficult to desorb from Ru/TiO_2 catalyst surface at temperature lower than 100 ^{o}C.

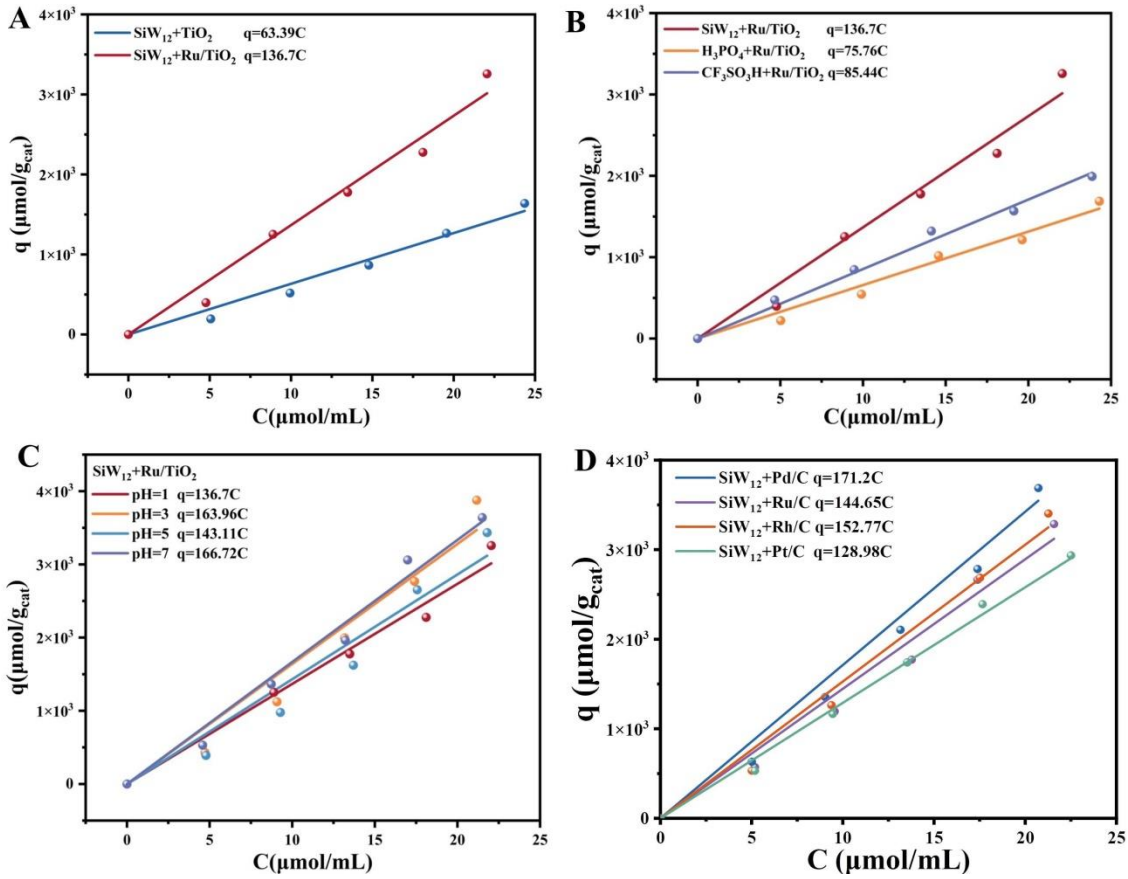

Supplementary Fig.S8 The adsorption isotherms needed in this work to calculate the amount of adsorbed ammonia during the reaction. (A) The adsorption isotherms were measured at room temperature in SiW_{12} solution suspended with Ru/TiO_2 or TiO_2 catalyst particles respectively; (B) The adsorption isotherms were measured at room temperature respectively in SiW_{12} solution, CF_3SO_3H solution and H_3PO_4 solution suspended with Ru/TiO_2 catalysts; (C) The adsorption isotherms were measured at room temperature in different pH values of SiW_{12} solution suspended with Ru/TiO_2 catalysts; (D) The adsorption isotherms were measured at room temperature in SiW_{12} solution suspended with different commercial carbon-supported metal catalysts.

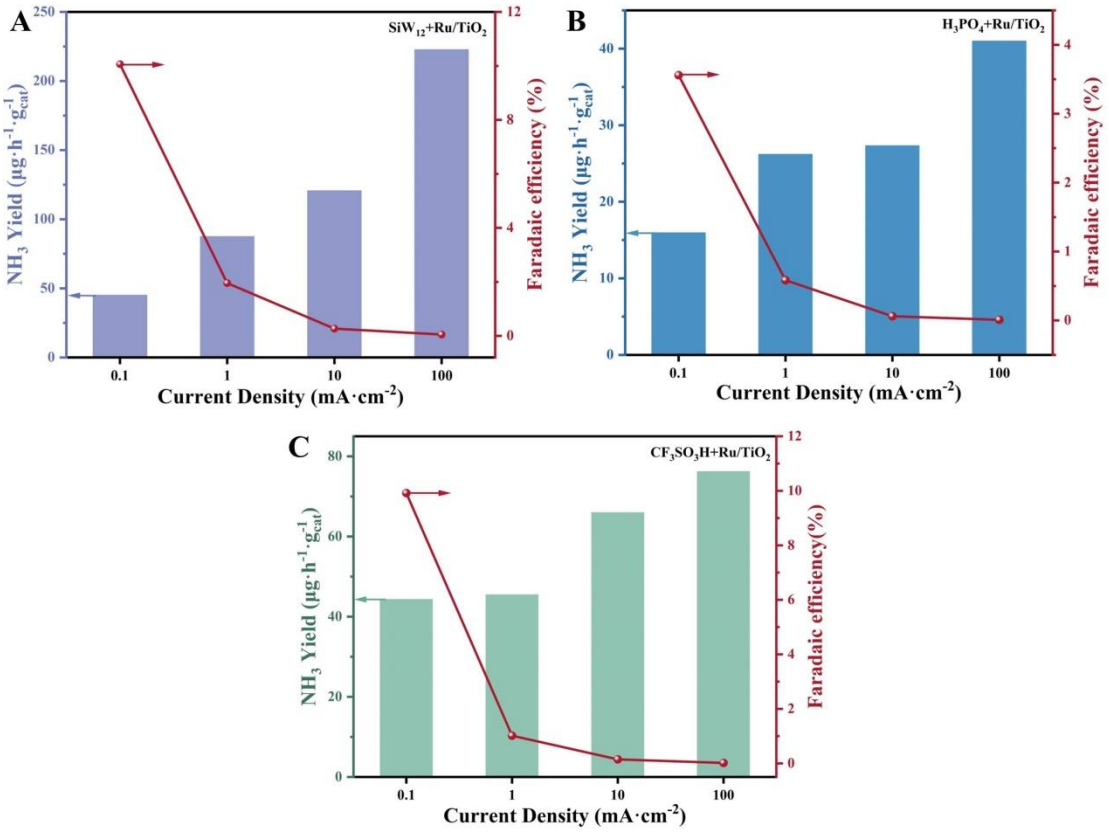

Supplementary Fig.S9 Ammonia yields and corresponding faradaic efficiency in different acid solutions (pH value is same with each other) under different electrolysis current densities and 10mL/min N_2. **(A)** Ammonia yields and corresponding faradaic efficiency at electrolysis 4h in SiW_{12} solution (0.5g SiW_{12}, 35mL H_2O) suspended with 0.05g Ru/TiO_2 catalysts. (**B**) Ammonia yields and corresponding faradaic efficiency at electrolysis 4h in H_3PO_4 solution suspended with 0.05g Ru/TiO_2 catalysts. (**C**) Ammonia yields and corresponding faradaic efficiency at electrolysis 4h in CF_3SO_3H solution suspended with 0.05g Ru/TiO_2 catalysts.

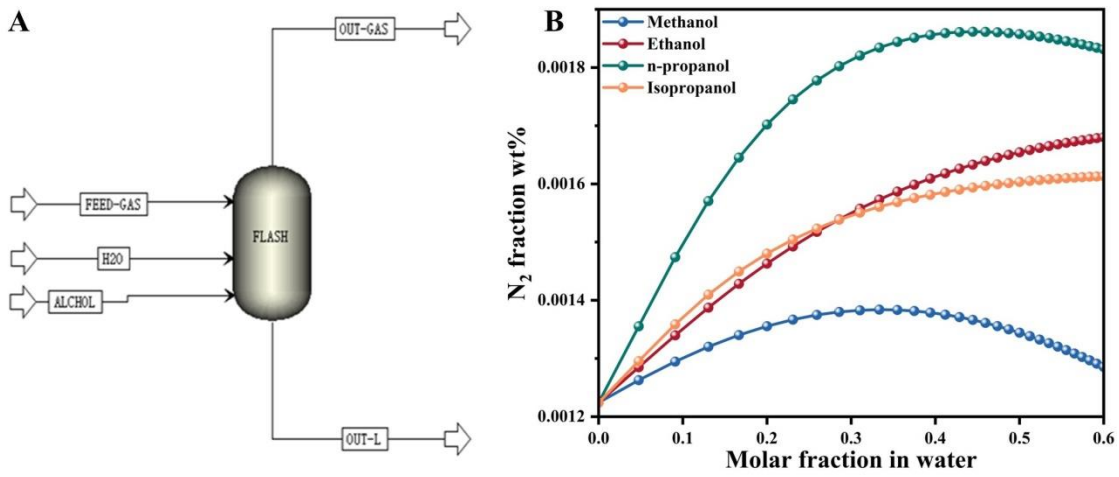

Supplementary Fig.S10 The nitrogen gas solubility in alcohol-water is calculated by software of Aspen Plus V11. **(A)** The two-phase flash model was built to calculate the nitrogen gas solubility in water with concentration of different alcohols. An activity coefficient-based model of "NRTL" (Non-Random-Two-Liquid) was applied for the property method. **(B)** The calculated nitrogen gas solubility in water with different alcohol concentrations.

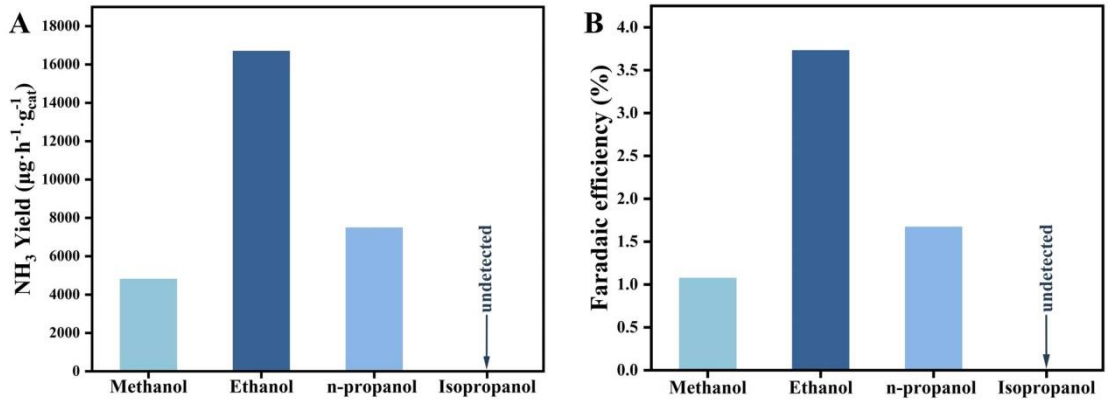

Supplementary Fig.S11 (A) The ammonia yields and (B) corresponding faradaic efficiency at electrolysis 4h in different alcohol-SiW_{12} aqueous solutions (0.5g SiW_{12}, 3mL alcohol, 32mL H_2O) suspended with 0.05g Ru/TiO_2 catalyst particles under constant electrolysis current density of 100 mA/cm^2 and 10mL/min N_2.

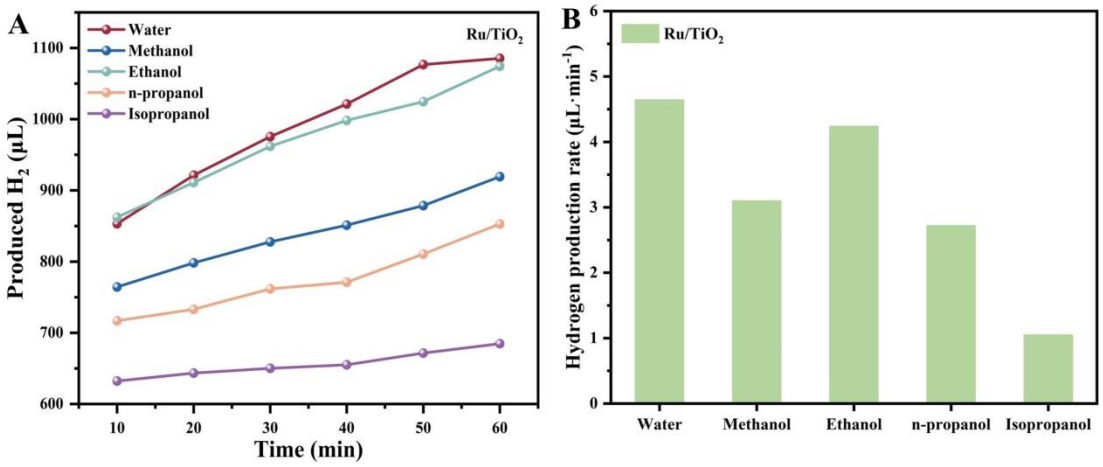

Supplementary Fig.S12 Electron release rate of SiW_{12} anion in different substances as solvent. SiW_{12} can transfer electrons from the cathode and then release electrons to reduce the protons for hydrogen H_2 gas generation over the suspended Ru/TiO_2 catalyst with a rather fast transfer rate. These processes could be described as

$$\left(SiW_{11}^{6}W^{5}O_{40}\right)^{5-} + H^{+} \xrightarrow{Ru/TiO_2} \left(SiW_{12}^{6}O_{40}\right)^{4-} + \frac{1}{2}H_2\uparrow$$

As seen, measuring the hydrogen H_2 production can estimate the electron release rate of SiW_{12} anion. Consequently, the electron release rate of SiW_{12} anion is estimated using hydrogen production rate. **(A)** and **(B)** are respectively the hydrogen H_2 gas volume *versus* time and production rate, which are measured when the electrolysis (current density is $100mA/cm^2$) of SiW_{12} solution for 10min and then electrolysis stopped. The SiW_{12} solution contains 3mL alcohols, 32mL H_2O and 0.05g Ru/TiO_2.

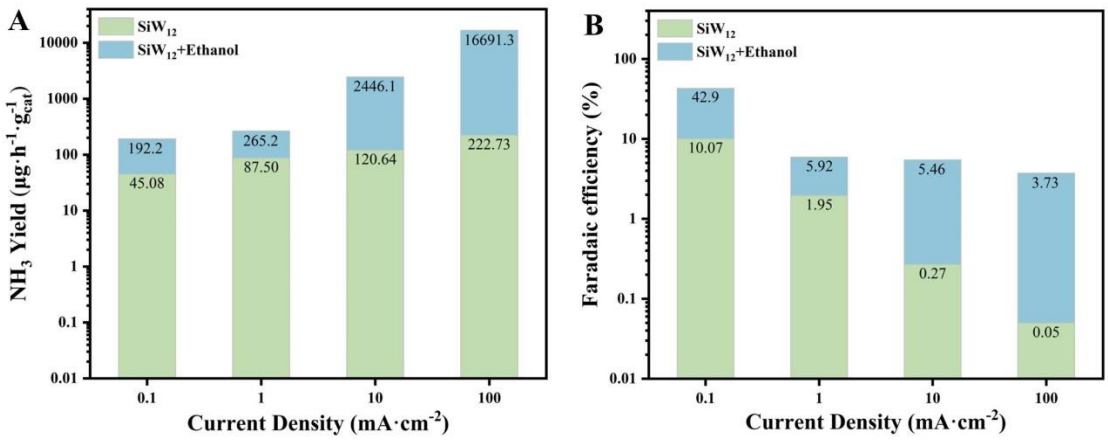

Supplementary Fig.S13 (A) The ammonia yields and (B) corresponding faradaic efficiency at electrolysis 4h in SiW_{12} aqueous solution (0.5g SiW_{12}, 35mL H_2O) and ethanol-SiW_{12} aqueous solution (0.5g SiW_{12}, 3mL ethanol, 32mL H_2O) suspended with 0.05g Ru/TiO_2 catalyst particles under different electrolysis current densities and 10mL/min N_2.

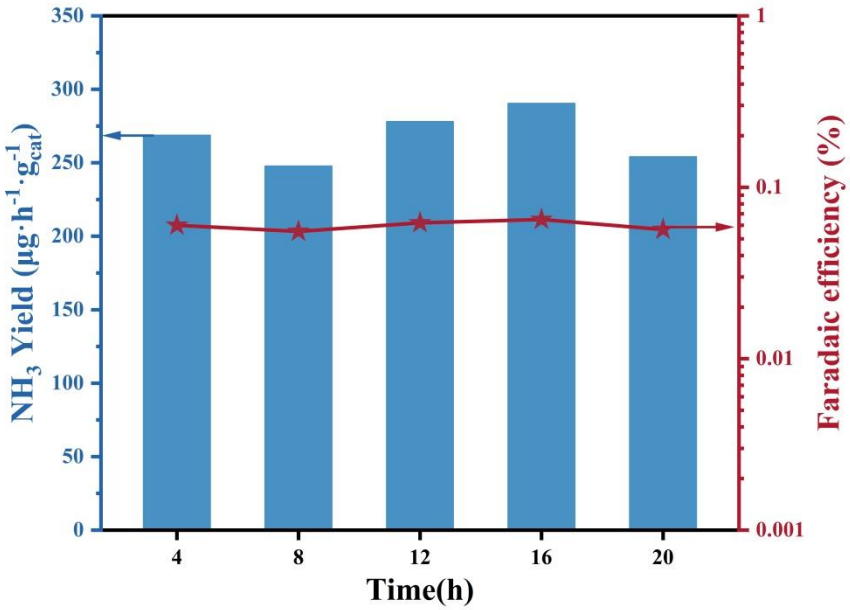

Supplementary Fig.S14 Stability of ammonia productions was tested in SiW_{12}-water solution (0.5g SiW_{12}, 35mL H_2O) suspended with 0.05g Ru/TiO_2 catalysts under a constant electrolytic current of 100 mA/cm^2 and 10mL/min N_2. The every cycle test period is four hours.

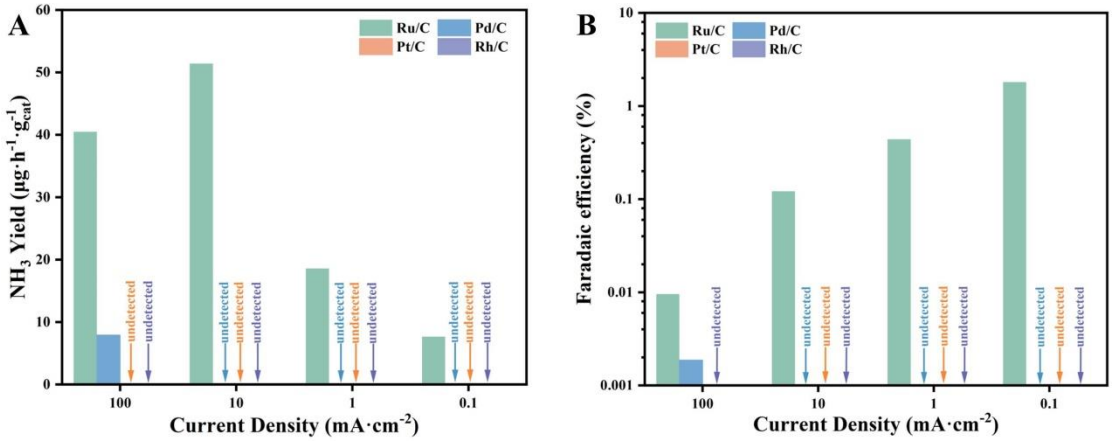

Supplementary Fig.S15 (**A**) The ammonia yields and (**B**) corresponding faradaic efficiency at electrolysis 4h in SiW_{12} aqueous solution (0.5g SiW_{12}, 35mL H_2O) suspended with different commercial carbon supported catalysts of Ru/C, Rh/C, Pt/C or Pd/C under different electrolysis current densities and 10mL/min N_2. The amount of catalyst particles used was 0.05g and 5wt% metal loading on carbon support.

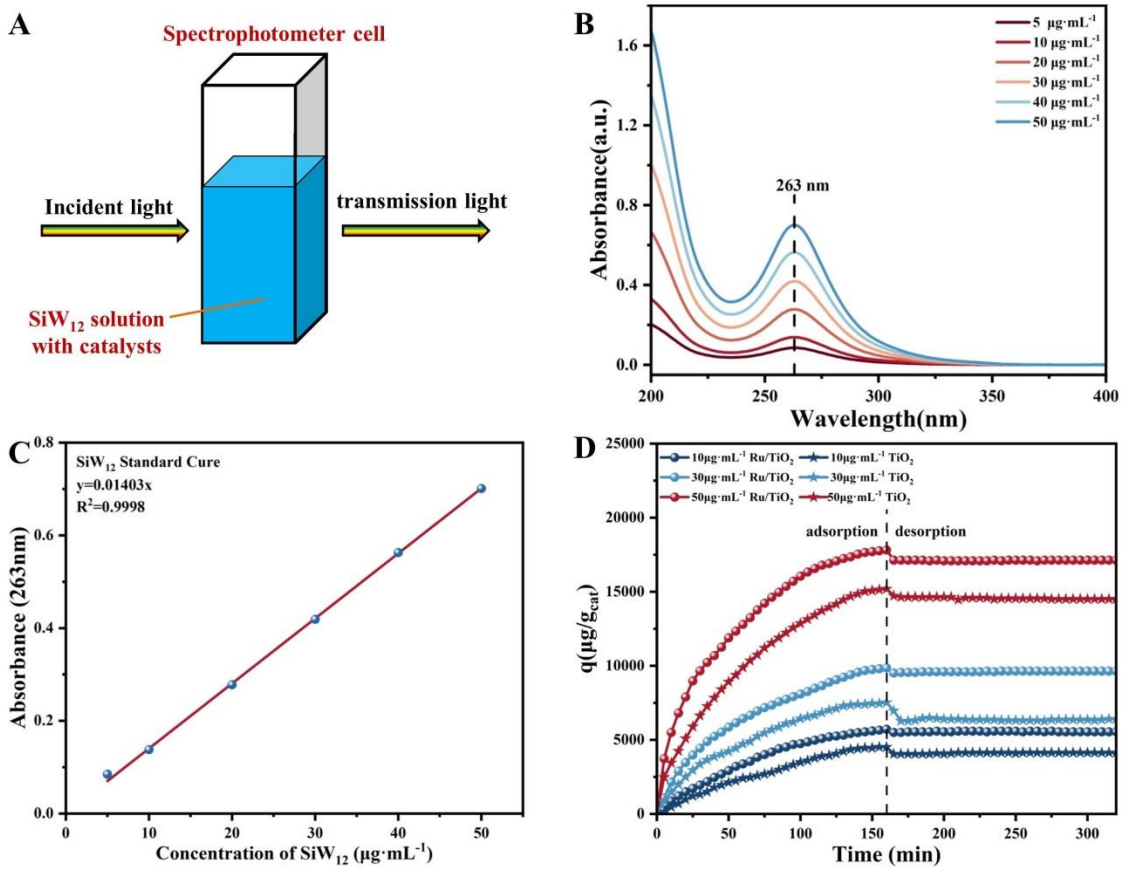

Supplementary Fig.S16 (A) Schematic diagram of UV-Vis spectrophotometer for *in sit*u measurements of SiW_{12} adsorption and desorption kinetics on Ru/TiO_2 or TiO_2 suspended in SiW_{12} aqueous solution. **(B)** The absorbance of SiW_{12} aqueous solution with different known SiW_{12} concentrations. **(C)** Standard curves of SiW_{12} solution correlating the absorbance with SiW_{12} concentrations. **(D)** Measured SiW_{12} adsorption and desorption kinetics curves on Ru/TiO_2 and TiO_2 respectively.

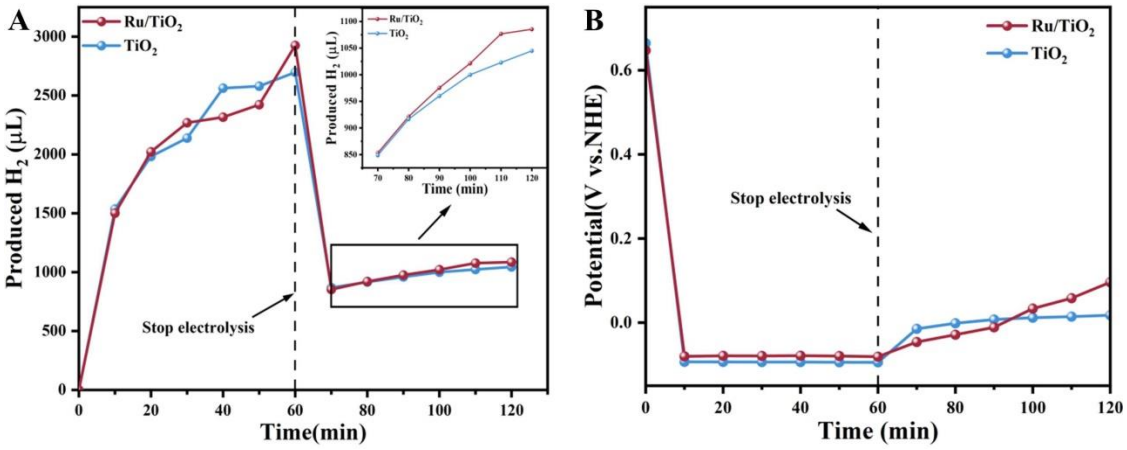

Supplementary Fig.S17 (A) Hydrogen H_2 gas evolution in SiW_{12} aqueous solution respectively suspended with Ru/TiO_2 and TiO_2 catalysts under a constant electrolytic current of 100 mA/cm^2 (before 60 min) and without electrolysis (after 60 min). **(B)** Electrode potential changes of SiW_{12} aqueous solution respectively suspended with Ru/TiO_2 and TiO_2 catalysts under a constant electrolytic current of 100 mA/cm^2 (before 60 min) and without electrolysis (after 60 min). Ag/AgCl electrode serve as counter electrode and reference electrode. In all above experiments, the amount of catalyst particles used was 0.05g and the SiW_{12} aqueous solution contained 35mL H_2O with 0.5g SiW_{12}.

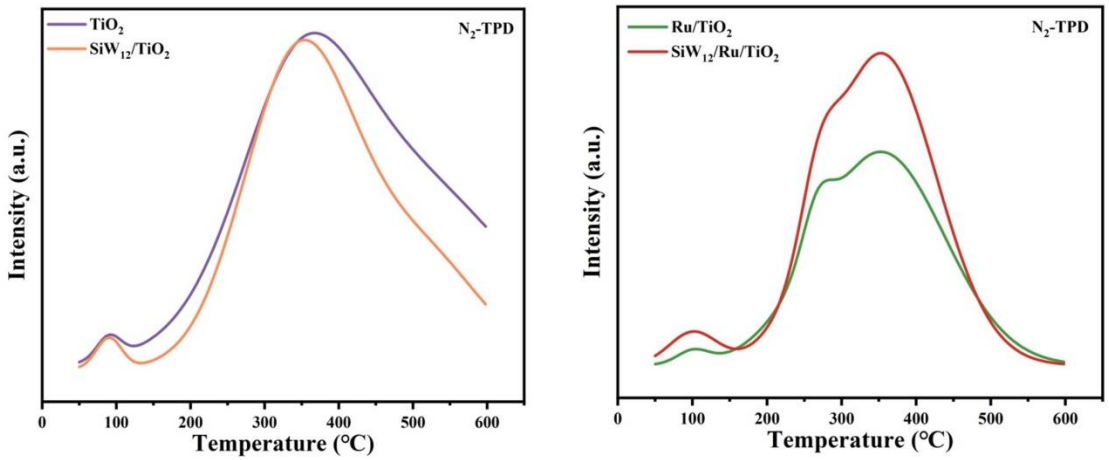

Supplementary Fig.S18 TPD spectra of N_2 from Ru/TiO_2, TiO_2, SiW_{12}/TiO_2 (TiO_2 adsorbed with SiW_{12}) and $SiW_{12}/Ru/TiO_2$ (Ru/TiO_2 adsorbed with SiW_{12}) catalysts after exposure to N_2 at 50^oC for 1h.

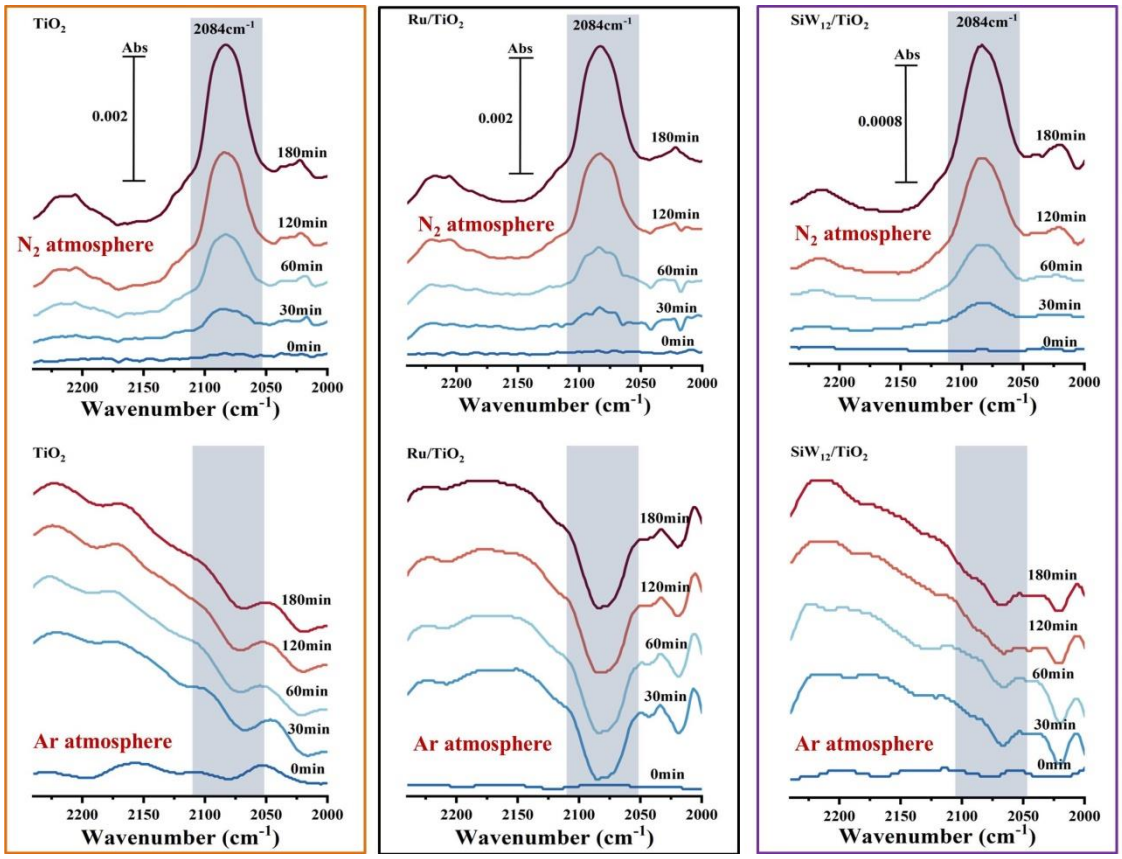

Supplementary Fig.S19 *In-situ* FT-IR spectra of N_2 molecules adsorbed on TiO_2, Ru/TiO_2 and SiW_{12}/TiO_2 (TiO_2 adsorbed with SiW_{12}) with time under ambient temperature and 1atm nitrogen atmosphere or 1atm argon atmosphere.

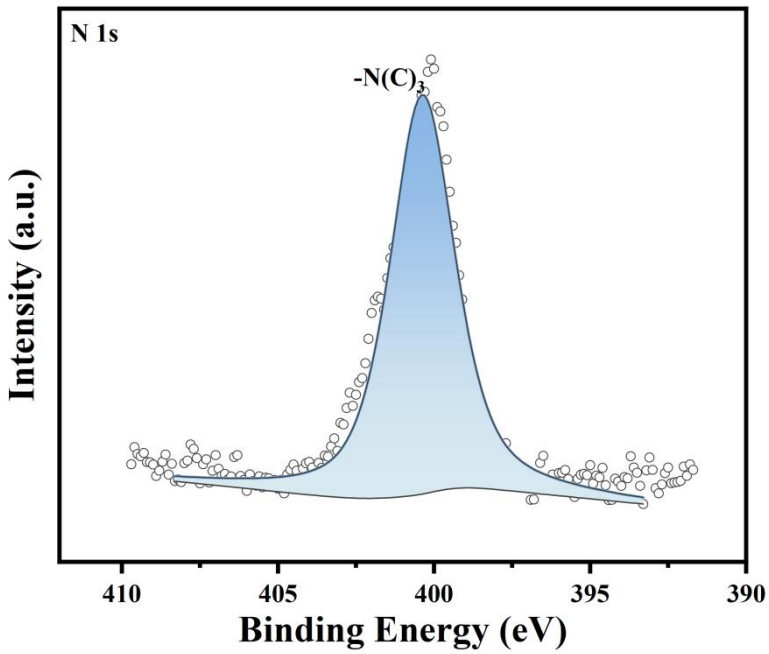

Supplementary Fig.S20 N 1s XPS spectra of Ru/TiO_2 in SiW_{12} aqueous solution after electrolysis 4h under 1atm argon Ar atmosphere (flow rate 10mL/min). Reaction solution volume is 35mL, and the aqueous solution contained 0.5g SiW_{12}, 35mL H_2O and 0.05g Ru/TiO_2. The electrolytic current density is 100 mA/cm^2.

N_2 hydrogenation in distal pathway

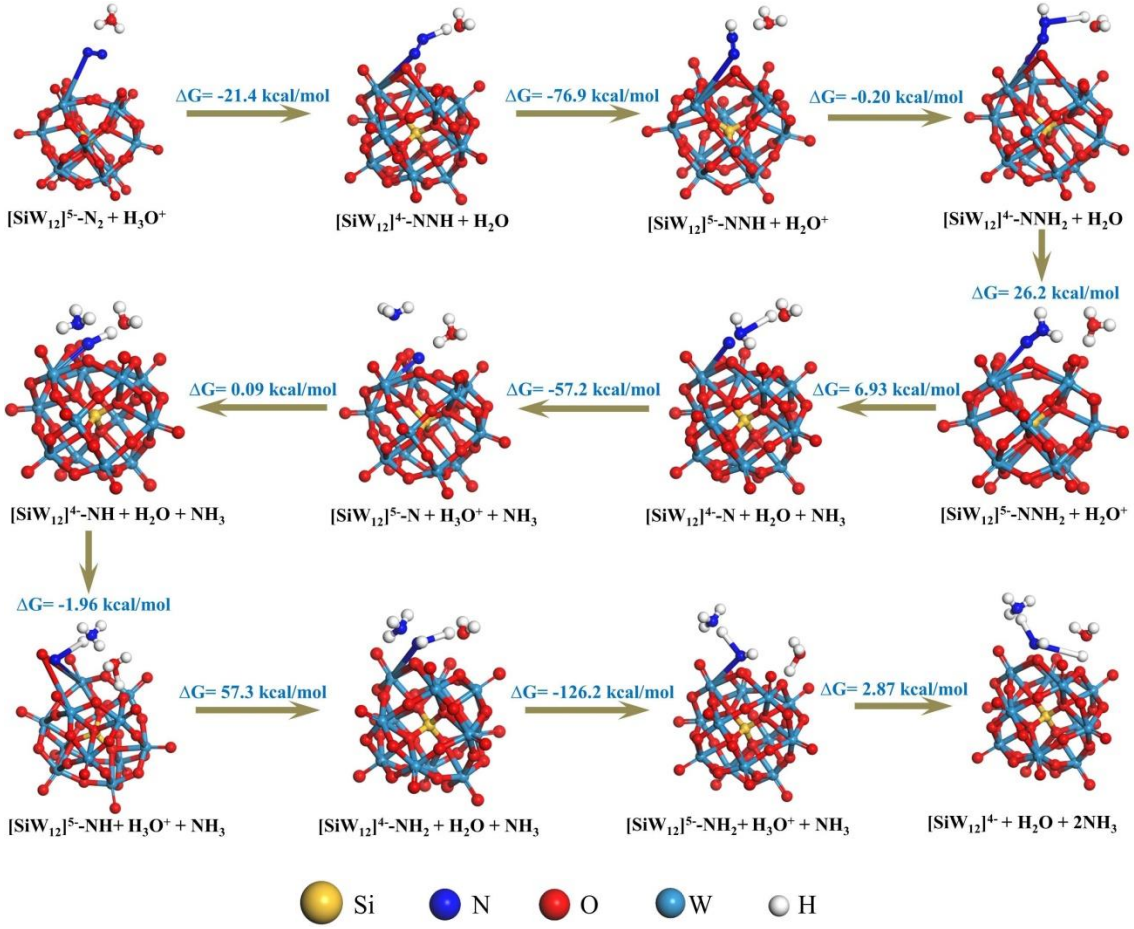

Supplementary Fig.S21 Most stable configurations and free energy profiles in DFT calculations for nitrogen hydrogenation on SiW_{12} in associative-distal pathway

N_2 hydrogenation in alternating pathway

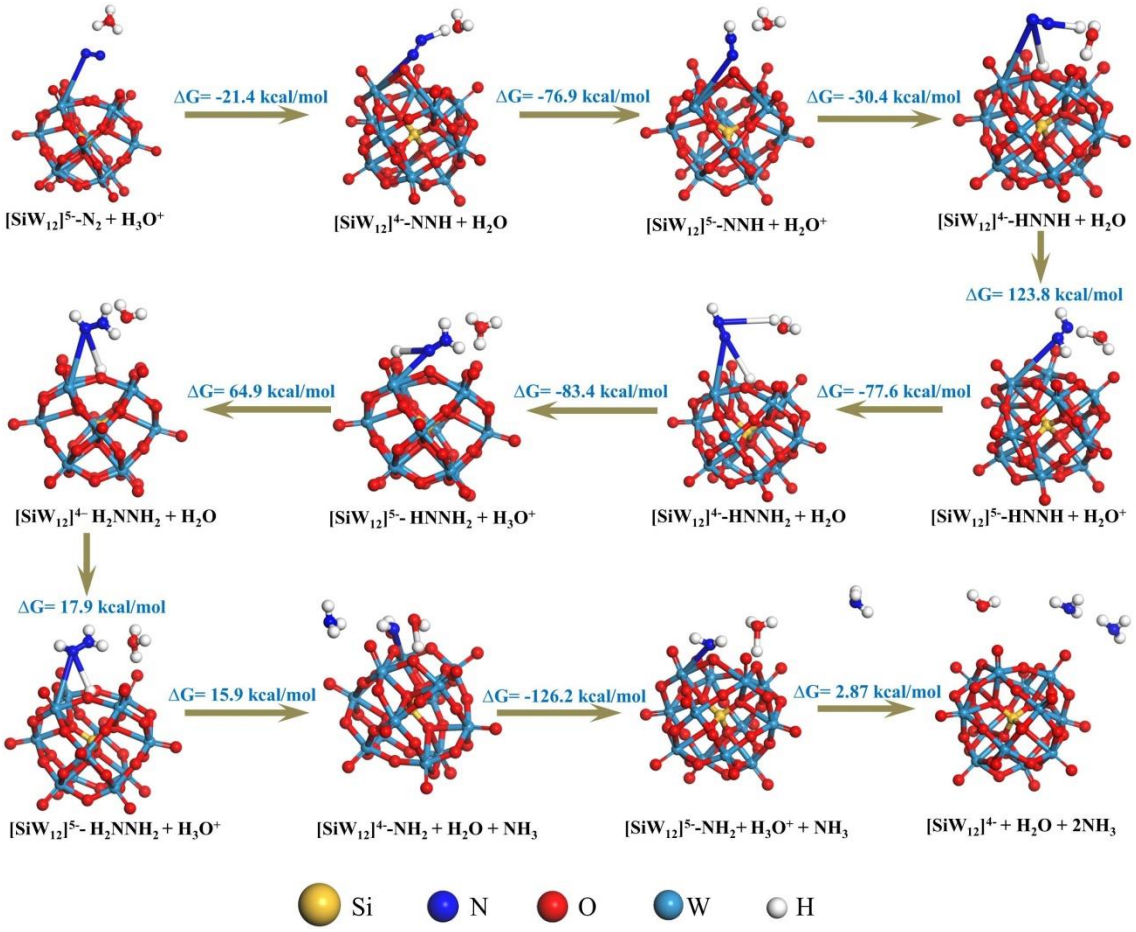

Supplementary Fig.S22 Most stable configurations and free energy profiles in DFT calculations for nitrogen hydrogenation on SiW_{12} in associative- alternating pathway

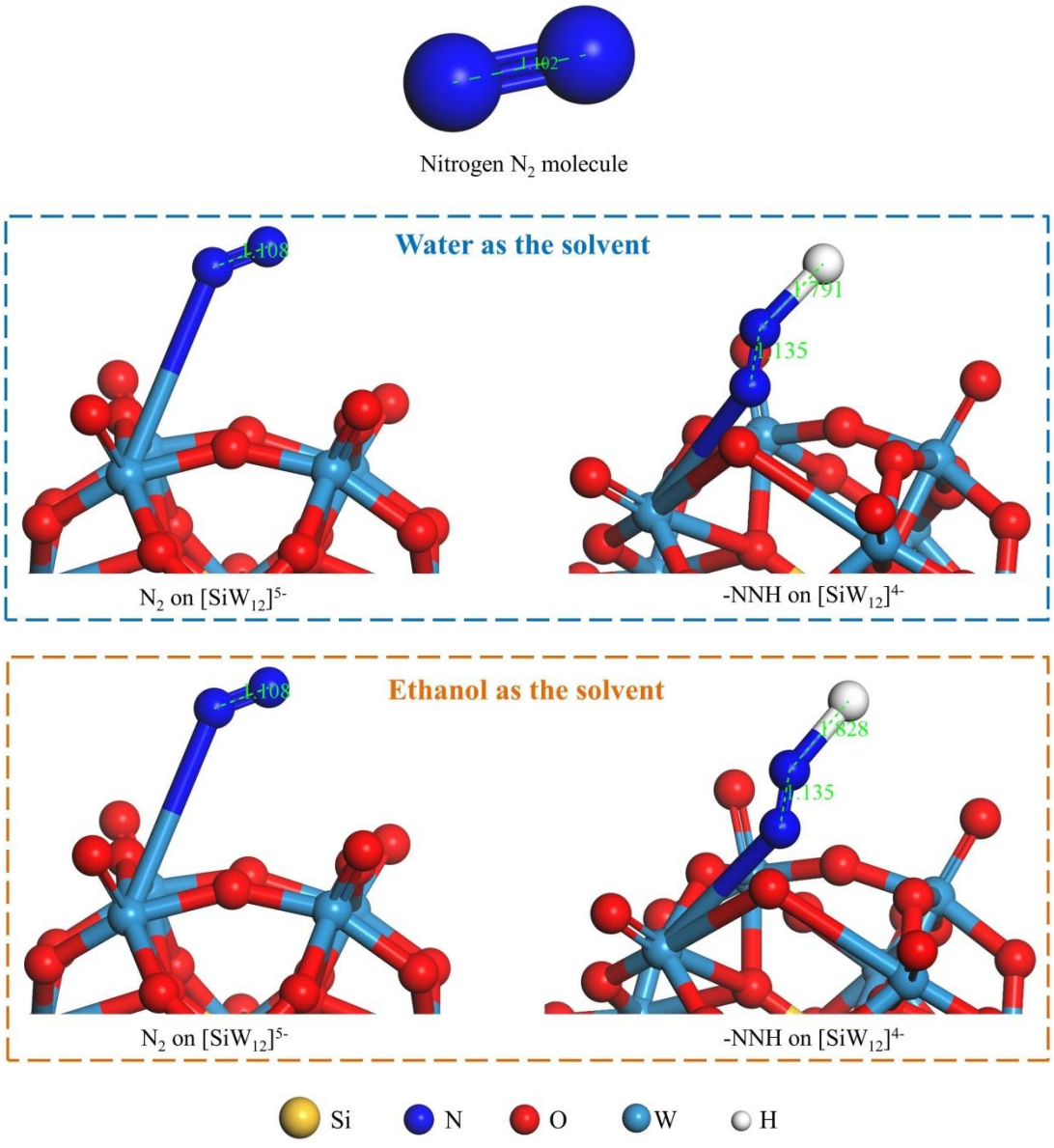

Supplementary Fig.S23 Most stable configurations of nitrogen N_2 in gas phase, N_2 on $[SiW_{12}]^{5-}$ and -NNH on $[SiW_{12}]^{4-}$ in DFT calculations, and the bond length unit is Å. The bond length of N≡N is calculated as 1.102 Å and is prolonged to be 1.108 Å on $[SiW_{12}]^{5-}$ in water or ethanol. The N=N bond length of -NNH is calculated as 1.135 Å in water or ethanol and the N-H bond length of -NNH is calculated as 1.791 Å and 1.828 Å respectively in water and ethanol.

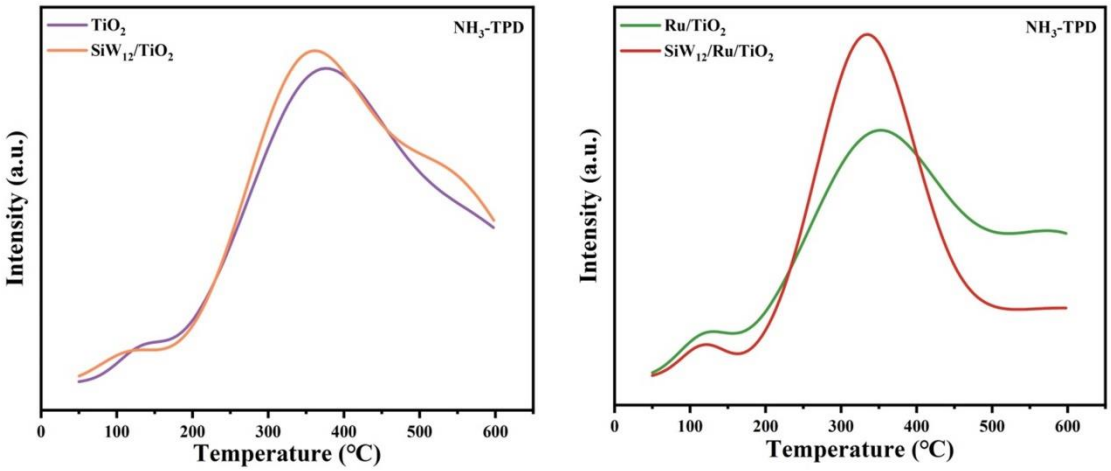

Supplementary Fig.S24 TPD spectra of NH_3 from Ru/TiO_2, TiO_2, SiW_{12}/TiO_2 (TiO_2 adsorbed with SiW_{12}) and $SiW_{12}/Ru/TiO_2$ (Ru/TiO_2 adsorbed with SiW_{12}) catalysts after exposure to NH_3 at 50^oC for 1h.

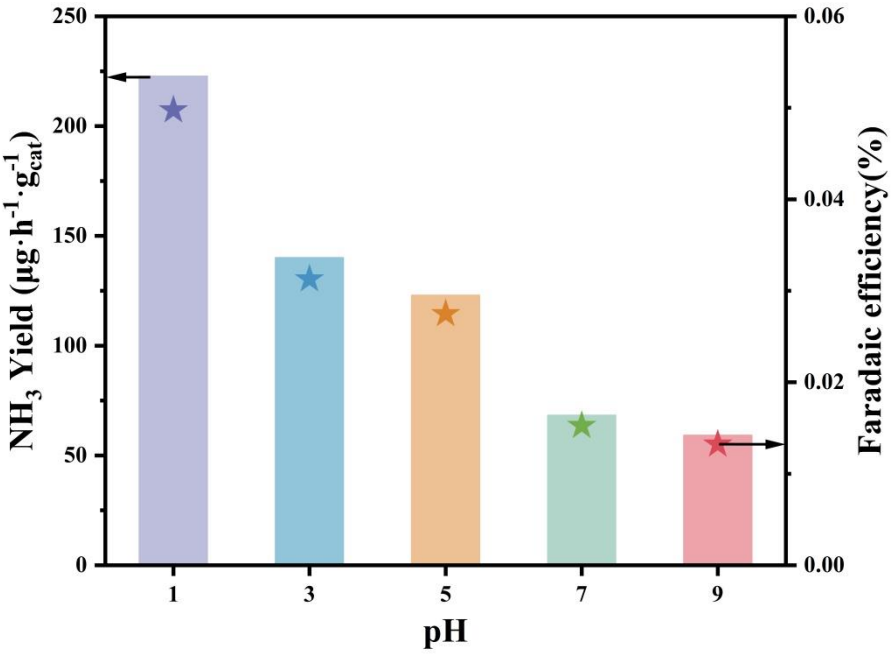

Supplementary Fig.S25 Ammonia production and corresponding Faradaic efficiency at electrolysis 4h in SiW_{12} solution suspended with Ru/TiO_2 under different pH conditions. Reaction solution: 0.5g SiW_{12}, 35mL H_2O and 0.05g Ru/TiO_2 catalysts. The electrolytic current density is 100 mA/cm^2 and the flow rate of nitrogen N_2 gas is 10mL/min.

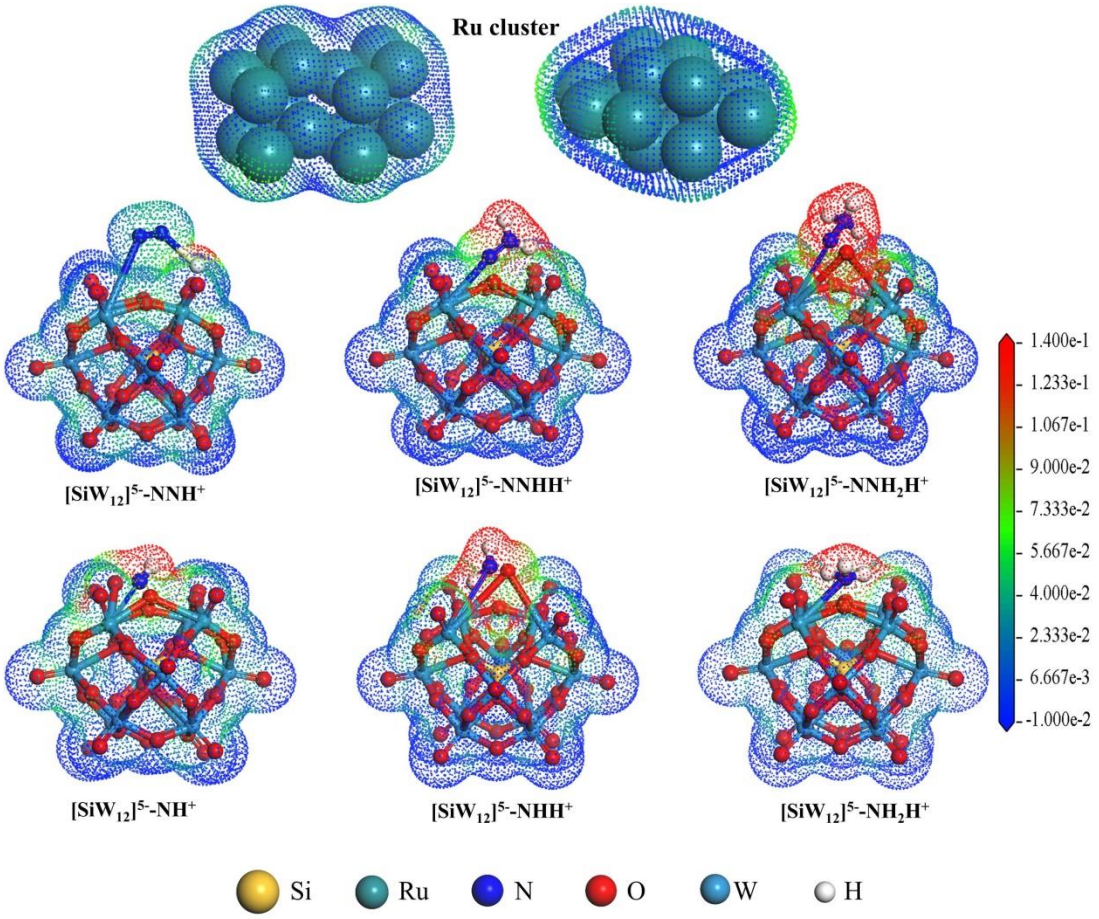

Supplementary Fig.S26 The electrostatic potentials profiles of Ru cluster and SiW_{12} with $[-NNH_n]^+$ or $[-NH_n]^+$ species. These are the most stable configurations calculated by DFT calculations. The Ru cluster has almost negative potential profiles around the surface of Ru cluster and the $[SiW_{12}]^{5-}$ anion also has the almost negative potential profiles. The $[-NNH_n]^+$ and $[-NH_n]^+$ show positive potential profiles, especially within the proton H^+ zone and the positive potentials are enhanced with the hydrogenation reaction proceeded. This indicates the Ru cluster could repel the electrons from SiW_{12} and $[-NNH_n]^+$ or $[-NH_n]^+$ could attract electrons from SiW_{12}, which further confirms the stored electron can be pushed from SiW_{12} by Ru clusters to the adsorbed nitrogen species.

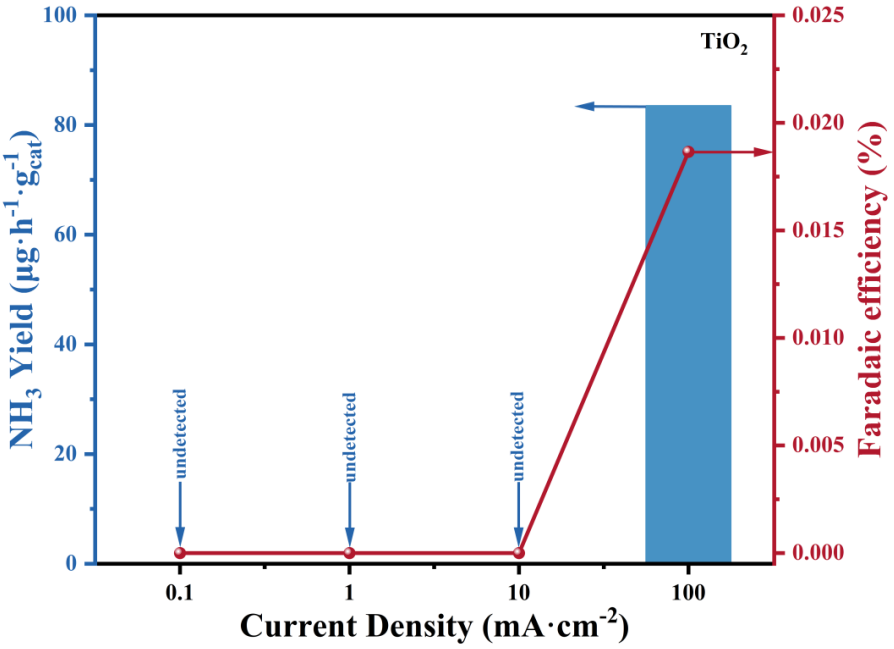

Supplementary Fig.S27 Ammonia production and corresponding Faradaic efficiency at electrolysis 4h in SiW_{12} solution suspended with only TiO_2 support under different current densities. Reaction solution: 0.5g SiW_{12}, 35mL H_2O and 0.05g TiO_2. The flow rate of nitrogen N_2 gas is 10mL/min.

Supplementary text

1. Structure characterizations of prepared Ru/TiO_2 catalyst

The X-ray diffraction (XRD) patterns of TiO_2 and Ru/TiO_2 catalysts are shown in Supplementary Fig.S28. As seen the catalysts exhibit characteristic peaks at 25.28°, 37.8°, 48.05°, and 55.06°, corresponding to the (101), (004), (200) and (211) crystal planes of the anatase structure of TiO_2 (PDF # 00-21-1272). In addition, the main peak of Ru/TiO_2 is slightly shifted to a lower diffraction angle compared to TiO_2, indicating that Ru elements are successfully incorporated into the TiO_2 lattice[43]. The Ru/TiO_2 catalyst has a Ru loading of 0.28wt% which is measured by inductively coupled plasma emission spectrometry (ICP-OES). The nitrogen N_2 low temperature adsorption-desorption isotherm gives the pore size distribution of catalysts as shown in Supplementary Fig.S28. As seen, TiO_2 has a specific surface area of 145.24 m^2/g, a pore volume of 0.287 cm^3/g and a mean pore size of 6.59 nm. Ru/TiO_2 has a specific surface area of 130.24 m^2/g, a pore volume of 0.271 cm^3/g and a mean pore size of 7.04nm. This indicates that the Ru loading does not change the pore structure of TiO_2.

SEM and TEM images reveal the morphology of TiO_2 and Ru/TiO_2 catalysts as shown in Supplementary Fig.S29. As seen, the Ru loading shows no effect on TiO_2 morphology. HRTEM analysis shows that Ru/TiO_2 nanoparticles have clearly visible lattice streaks, indicating that Ru/TiO_2 nanoparticles have high crystallinity. Analysis by Fast Fourier transform (FFT) technique shows that the lattice fringe spacing of Ru/TiO_2 nanoparticles is 0.348nm which ascribes to the (101) crystal plane of anatase TiO_2, and 0.22 nm lattice fringe spacing which corresponds to the (111) crystal plane

of Ru[44,45]. In addition, the EDS elemental analysis diagram confirms the Ru element is evenly distributed on the TiO_2 support.

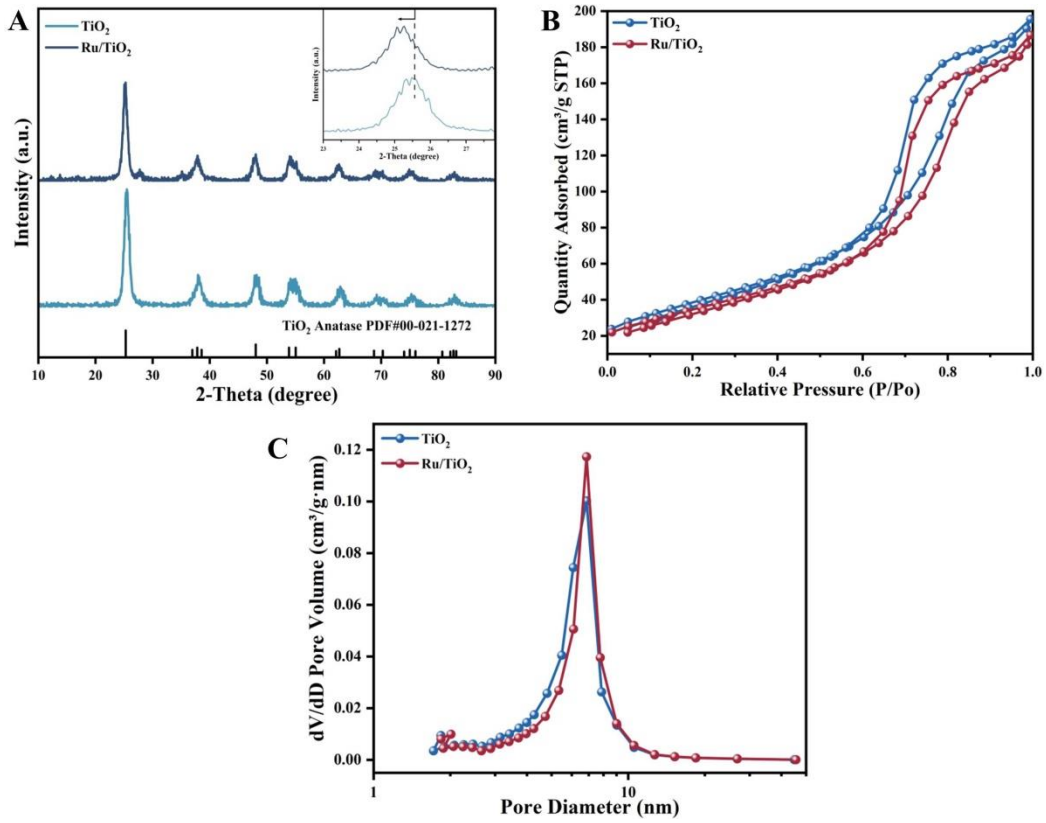

Supplementary Fig.S28 (A) XRD patterns of TiO_2 and Ru/TiO_2; (B) Nitrogen N_2 gas adsorption-desorption isotherms; (C) Pore size distributions of TiO_2 and Ru/TiO_2.

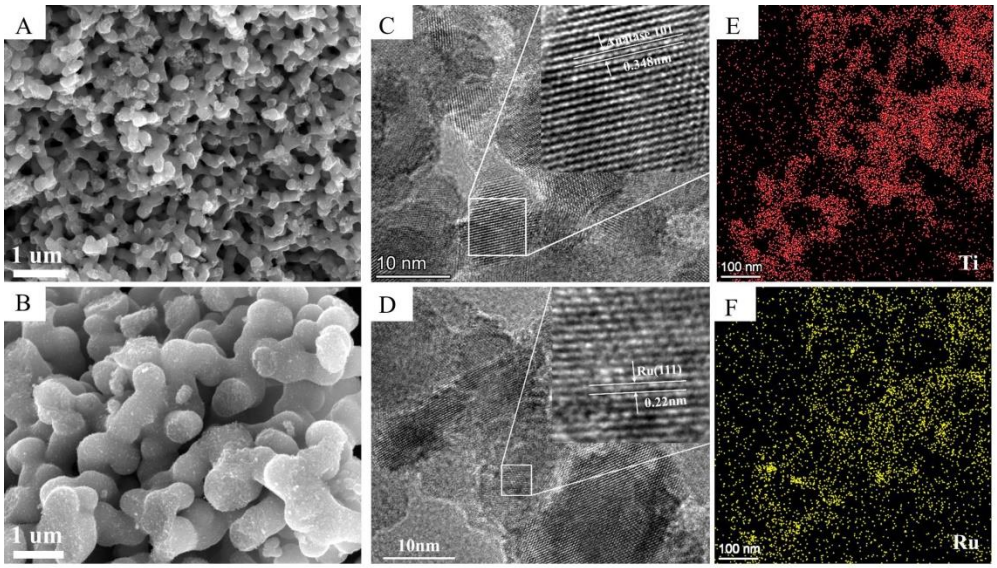

Supplementary Fig.S29 SEM images of (A) TiO_2 and (B) Ru/TiO_2; (C) and (D) are HRTEM images of Ru/TiO_2; (E) and (F) are EDS analysis diagram of Ru/TiO_2

The surface composition and element state of Ru/TiO_2 were further investigated by X-ray photoelectron spectroscopy (XPS) as shown in Supplementary Fig.S30. XPS spectra show that Ru/TiO_2 contain Ru, Ti and O elements. The peaks observed at 458.65 and 464.35 eV in the Ti 2p and Ru 3p spectra also match well with Ti^{4+} $2p_{3/2}$ and Ti^{4+} $2p_{1/2}$ [46,47], and the peaks at 472.13 and 477.35 eV are correlated with the satellite peaks of Ti[48]. The peaks at 461.18 and 483.18 eV in Ru 3p spectra are attributed to Ru $3p_{3/2}$ and Ru $3p_{1/2}$ respectively, suggesting that Ru species exist in a metallic state[49,50]. The O 1s spectra show lattice oxygen (O_L, 529.85 eV) , Ru-O-Ti (531.3eV) and adsorbed water (O_C, 533.2 eV)[51].

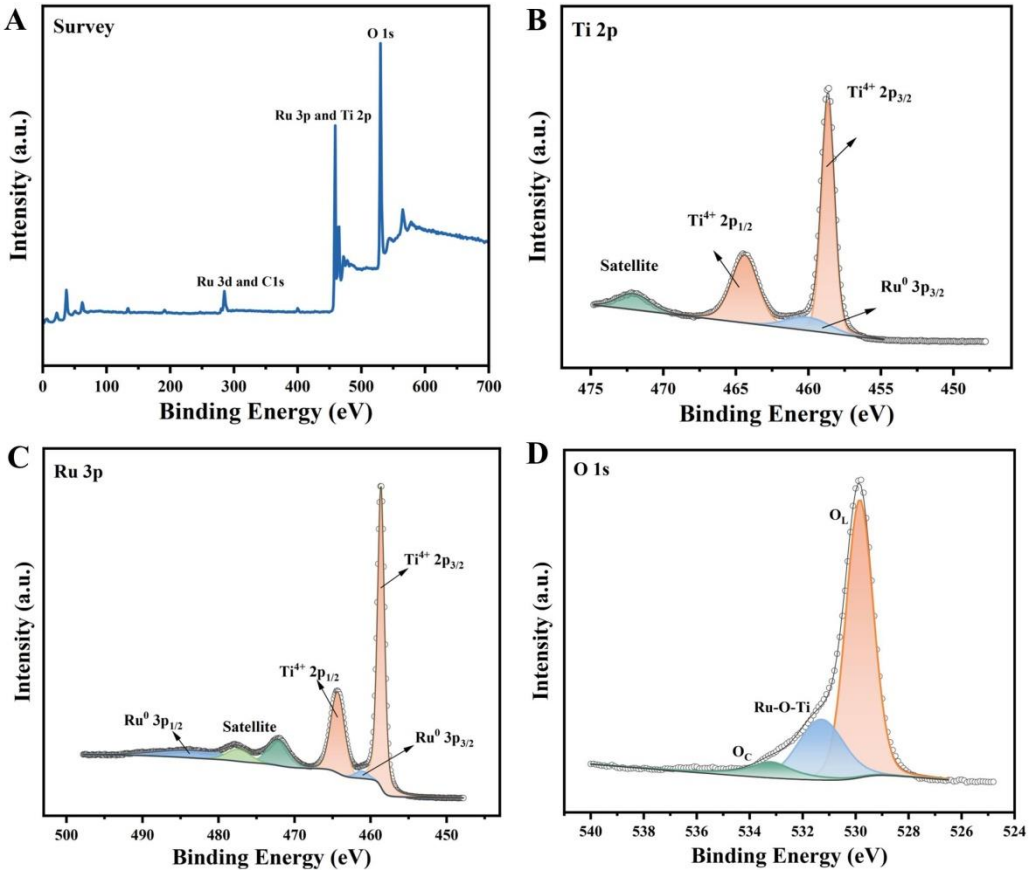

Supplementary Fig.S30 High-resolution XPS spectra of Ru/TiO_2: (A) full spectrum; (B) Ti 2p; (C) Ru 3p; (D) O 1s.

2. How the alcohols added in SiW_{12} solution affect the ammonia production

In our proposed electrochemical system, the reaction for nitrogen hydrogenation into ammonia is

$$N_2 + 6\left(SiW_{11}^{6}W^{5}O_{40}\right)^{5-} + 6H^{+} \xrightarrow{Ru/TiO_2} 6\left(SiW_{12}^{6}O_{40}\right)^{4-} + 2NH_3$$

The catalyst Ru/TiO_2 is prepared and its pore size is around 7nm which is much larger than nitrogen size 0.364nm. SiW_{12} is a relative large molecule with size of 1.08nm. Therefore, the nitrogen diffusion is not restrictive in pores of Ru/TiO_2 catalyst. But the SiW_{12} diffusion needs to be considered. Now let us consider the SiW_{12} mass balance in a spherical Ru/TiO_2 catalyst particle suspended in SiW_{12} solution as show in Supplementary Fig.S31. To simplify, the capital letter A is used to denote the SiW_{12} molecule.

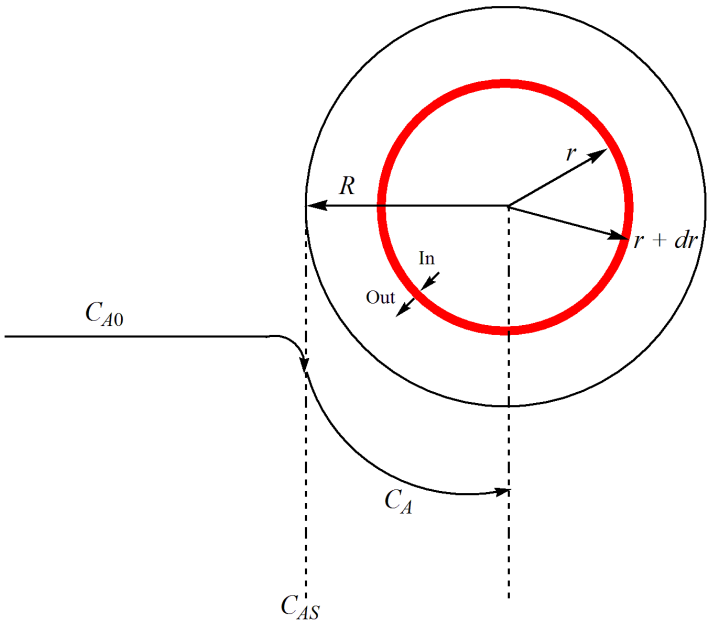

Supplementary Fig.S31 Schematic diagram of SiW_{12} mass balance in a spherical Ru/TiO_2 catalyst particle.

C_{A0} represents the SiW_{12} concentration in bulk solution; C_{AS} denotes the SiW_{12} concentration on catalyst surface; C_A is the SiW_{12} concentration within catalyst

particle; R is the radius of catalyst particle; r is the coordinate of SiW_{12} molecule within catalyst particle. The mass balance of SiW_{12} in an arbitrary spherical shell of catalyst particle is described as

$$\text{In (at } r\text{)} - \text{Out } (r + dr) + \text{Generation (within } dr\text{)} = 0$$

$$N_{\mathrm{A}} \cdot 4\pi r^2\Big|_{r} - N_{\mathrm{A}} \cdot 4\pi r^2\Big|_{r+\Delta r} + r_{\mathrm{A}} S\rho 4\pi r_m^2 \Delta r = 0 \tag{S-1}$$

where the N_{A} represents the diffusing flux of SiW_{12}; r_{A} is the reaction rate based on the catalyst surface; S is the surface area per unit mass of catalyst; ρ is the mass density of catalyst; r_m represents the mean radius of spherical shell. When $\Delta r \to 0$, the equation (S-1) becomes

$$\frac{d(N_{\mathrm{A}} r^2)}{dr} - r_{\mathrm{A}} S\rho r^2 = 0 \tag{S-2}$$

According to Fick's law, the N_{A} can be described as

$$N_{\mathrm{A}} = -D_e \frac{dC_{\mathrm{A}}}{dr} \tag{S-3}$$

D_e is the effective diffusivity of SiW_{12}. The reaction rate can be estimated using a power function as

$$r_{\mathrm{A}} = -k_i C_{\mathrm{A}}^n C_B^m C_C^q \tag{S-4}$$

k_i is the reaction constant; m, n and q denoted the reaction orders; C_{B} denotes the nitrogen N_2 concentration, that is nitrogen gas solubility. C_{C} denotes the proton H^+ concentration. In our electrolytic system, the nitrogen N_2 concentration in solution is constant under a given experimental conditions and the proton H^+ concentration is rather large. Then the equation (S-4) can be simplified as

$$r_{\mathrm{A}} = -k C_{\mathrm{A}}^n \tag{S-5}$$

where $k = k_i C_{\mathrm{B}}^m C_{\mathrm{C}}^q$.

Substituting equations (S-3) and (S-5) into (S-2), we can obtain

$$D_e \frac{1}{r^2}\frac{d}{dr}(r^2 \frac{dC_A}{dr}) - kS\rho C_A^n = 0 \quad \text{(S-6)}$$

Let $\psi = C_A/C_{AS}$, $\lambda = r/R$, the equation (S-6) becomes

$$\frac{1}{\lambda^2}\frac{d}{d\lambda}(\lambda^2 \frac{d\psi}{d\lambda}) - \frac{kS\rho R^2 C_{AS}^{n-1}}{D_e}\psi^n = 0 \quad \text{(S-7)}$$

Define the Thiele modulus ϕ_n as

$$\phi_n^2 = \frac{kS\rho R^2 C_{AS}^{n-1}}{D_e} \quad \text{(S-8)}$$

For nitrogen hydrogenation into ammonia, the reaction order for nitrogen is usually as ~1 and assuming the reaction order for SiW_{12} is one. Therefore, the equation (S-7) can be solved as

$$\psi = \frac{C_A}{C_{AS}} = \frac{1}{\lambda}\left(\frac{\sinh\phi_1\lambda}{\sinh\phi_1}\right) \quad \text{(S-9)}$$

Define the internal effective factor η as

$$\eta = \frac{\text{Actual overall rate of reaction}}{\text{Rate of reaction is when entire interior surface were exposed to the external pellet surface}} \quad \text{(S-10)}$$

The internal effective factor η can be expressed as

$$\eta = \frac{3}{\phi_1^2}(\phi_1 \coth\phi_1 - 1) \quad \text{(S-11)}$$

where

$$\phi_1 = \sqrt{\frac{kS\rho R^2}{D_e}} \quad \text{(S-12)}$$

As seen, the internal effective factor η is a monotonically decreasing function versus Thiele modulus ϕ_1 which is also a function of reaction rate and diffusion rate. It is found that the presence of alcohol in SiW_{12} solution could not only change the rate of

electron release of SiW_{12} anion, but also change the diffusion rate of SiW_{12} as shown in Supplementary Fig.S32.

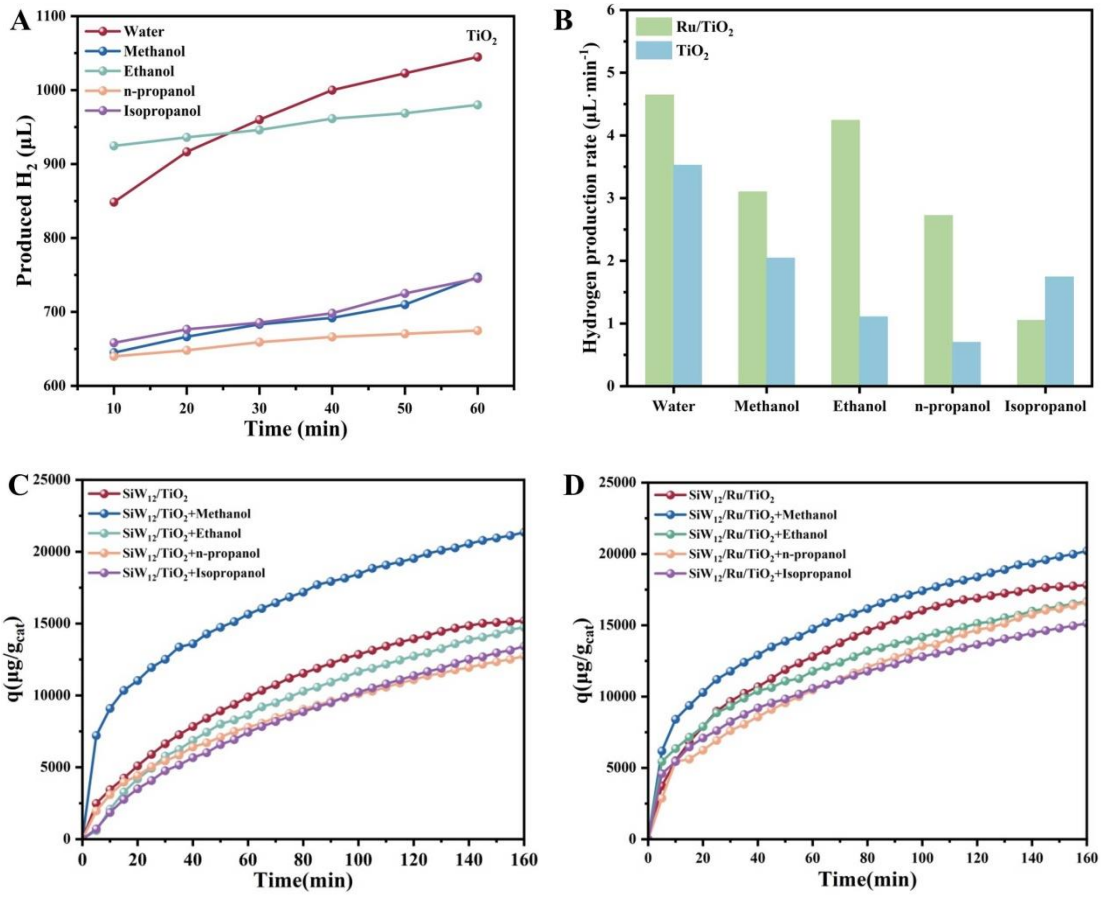

Supplementary Fig.S32 (A) Hydrogen H_2 volume *versus* time on TiO_2 are measured when the electrolysis (current density is 100mA/cm^2) of SiW_{12} solution for 10min and then electrolysis stopped (SiW_{12} solution contains 3mL alcohols, 32mL H_2O and 0.05g TiO_2). The hydrogen H_2 volume *versus* time on Ru/TiO_2 can be found in *Supplementary Fig.S12A.* (B) Electron release rate is estimated using the hydrogen H_2 production rate calculated from the data of hydrogen H_2 volume *versus* time. (C) and (D) are adsorption kinetics curves of SiW_{12} respectively on the Ru/TiO_2 and TiO_2 measured in aqueous solution with SiW_{12} concentration of 50ug/mL and alcohol concentration of 0.088mL/mL.

3. How the alcohols affect the ammonia determination by Nessler's reagents

In order to estimate the effects of water-soluble alcohols added into the reaction solution on the ammonia ion determination by Nessler's reagents. 3 mL alcohols were added into 32 mL water to get alcohol-water solution. Then 1 mL solution was taking out and added into 4 mL water to obtain 5 mL dilute alcohol-water solution. Finally, 0.2 mL Nessler's reagents were added into the 5 mL dilute alcohol-water solution to conduct UV-Vis spectroscopy measurements. As shown in Supplementary Fig.S33, absorbance with or without alcohols are almost same with each other, indicating that adding 3 mL alcohols into 32 mL water shows no effect the ammonia determination by Nessler's reagents.

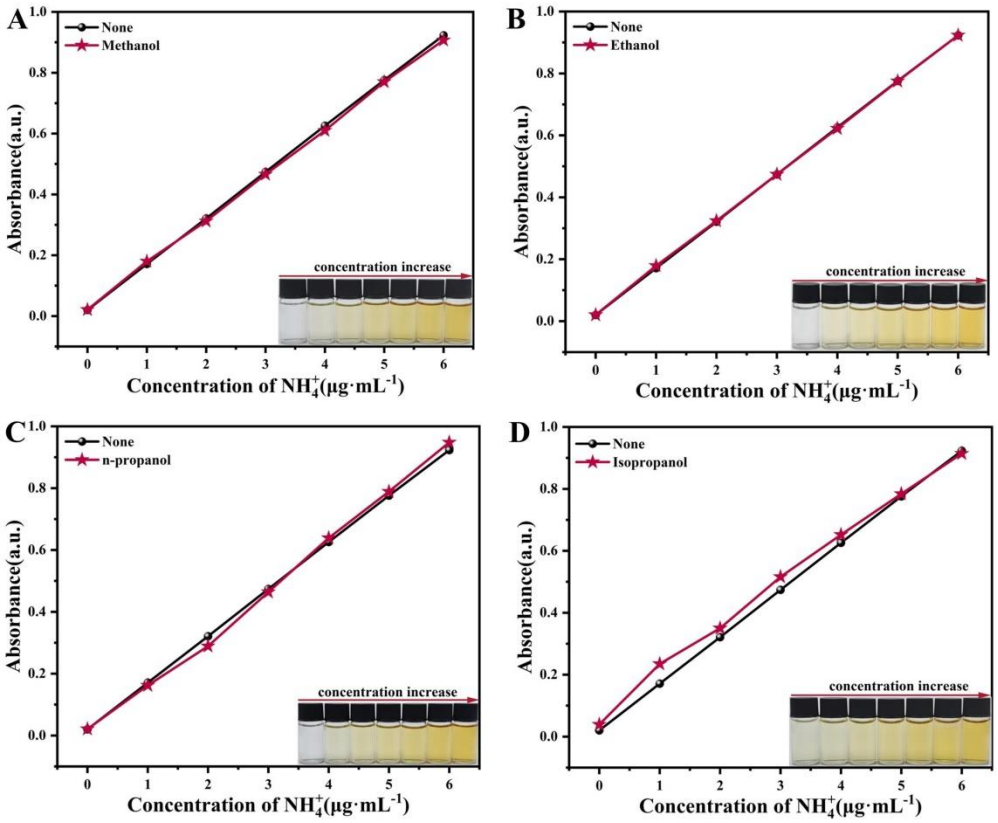

Supplementary Fig.S33 The UV-Vis absorbance of aqueous solution with different concentrations of NH_4^+ without or with different alcohols: (A) methanol, (B) ethanol, (C) n-propanol and (D) isopropanol.

4. Comparison of ammonia determination by ^{1}H-NMR or ion chromatography method with the colorimetric method of Nessler's reagents

The isotope experiments using $^{15}N_2$ as the feeding nitrogen gas are quantitatively analyzed to validate the yield rate of the detected ammonia. In order to compare, the colorimetric method was also used to test ammonia using $^{15}N_2$ as the feeding nitrogen gas. As shown in Supplementary Fig.S34, the ammonia in a sample reaction solution was determined respectively as 8.35 ug/mL by Nessler' reagents and 7.43 ug/mL by ^{1}H-NMR spectra. Furthermore, the ion chromatography was also used to verify the amount of ammonia produced and compared with the colorimetric method. As shown in Supplementary Fig.S35, the ammonia in a sample reaction solution was determined respectively as 1.39 ug/mL by ion chromatography and 1.27 ug/mL by colorimetric method of Nessler' reagents. These comparable values of ammonia produced with different methods indicate that the ammonia produced in our work could be accurately measured using colorimetric method. Hence, the colorimetric method of UV-Vis spectroscopy through the colorimetric reactions of Nessler's reagents was applied to quantify ammonia product in this work, due to its characteristic of accurate and easy quantification.

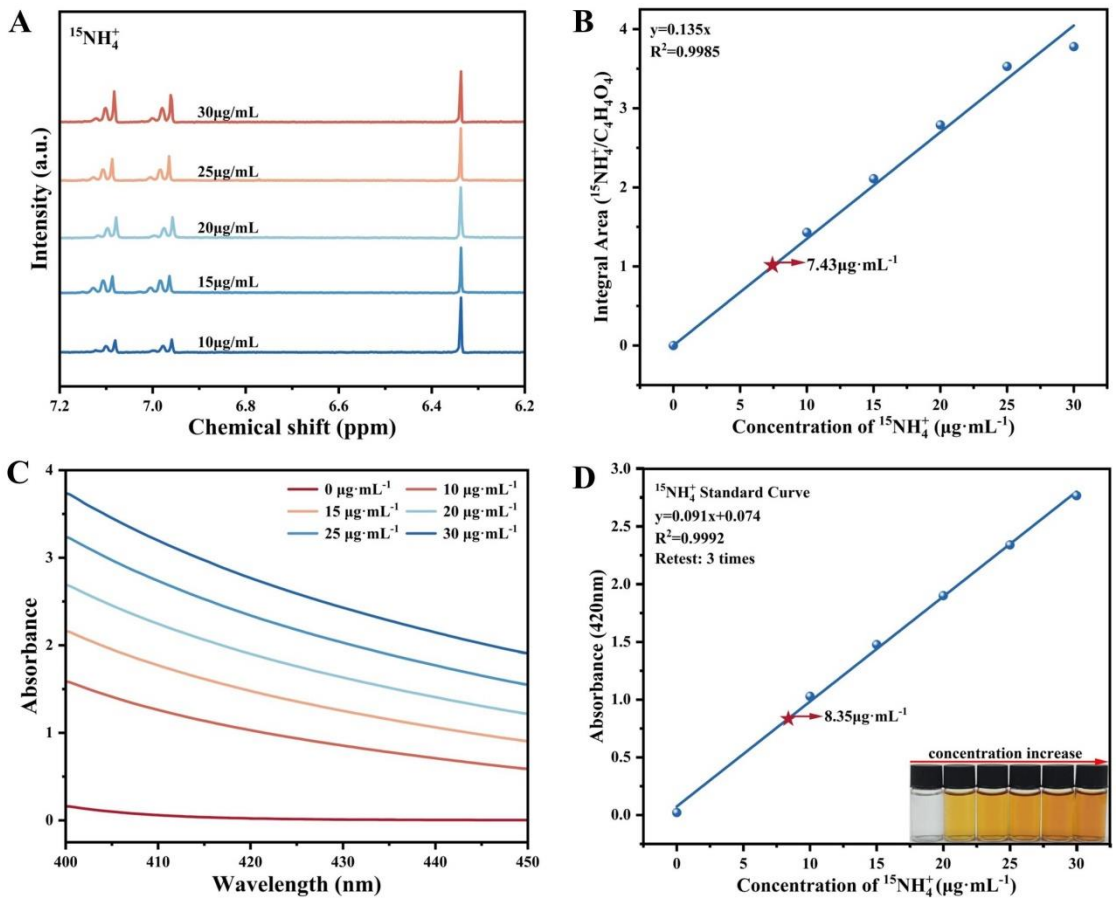

Supplementary Fig.S34 Electrocatalysis of nitrogen to ammonia using isotopic labeling $^{15}N_2$ as nitrogen gas feedstock. (A) NMR intensity of $^{15}NH_4Cl$ with different concentrations. The maleic acid, $C_4H_4O_4$, was used as the internal standard substance to give calibration curve. (B) Calibration curves for $^{15}NH_4Cl$ are based on peak area of NMR intensity. (C) UV-Vis absorbance of $^{15}NH_4Cl$ aqueous solutions with known $^{15}NH_4Cl$ concentrations. (D) Standard curve of the absorbance at 420 nm of $^{15}NH_4Cl$ aqueous solutions with different $^{15}NH_4Cl$ concentrations. The ammonia in a sample reaction solution (denoted by asterisk on curve) was determined respectively as 8.35 ug/mL by Nessler' reagents and 7.43 ug/mL by ^{1}H-NMR spectra.

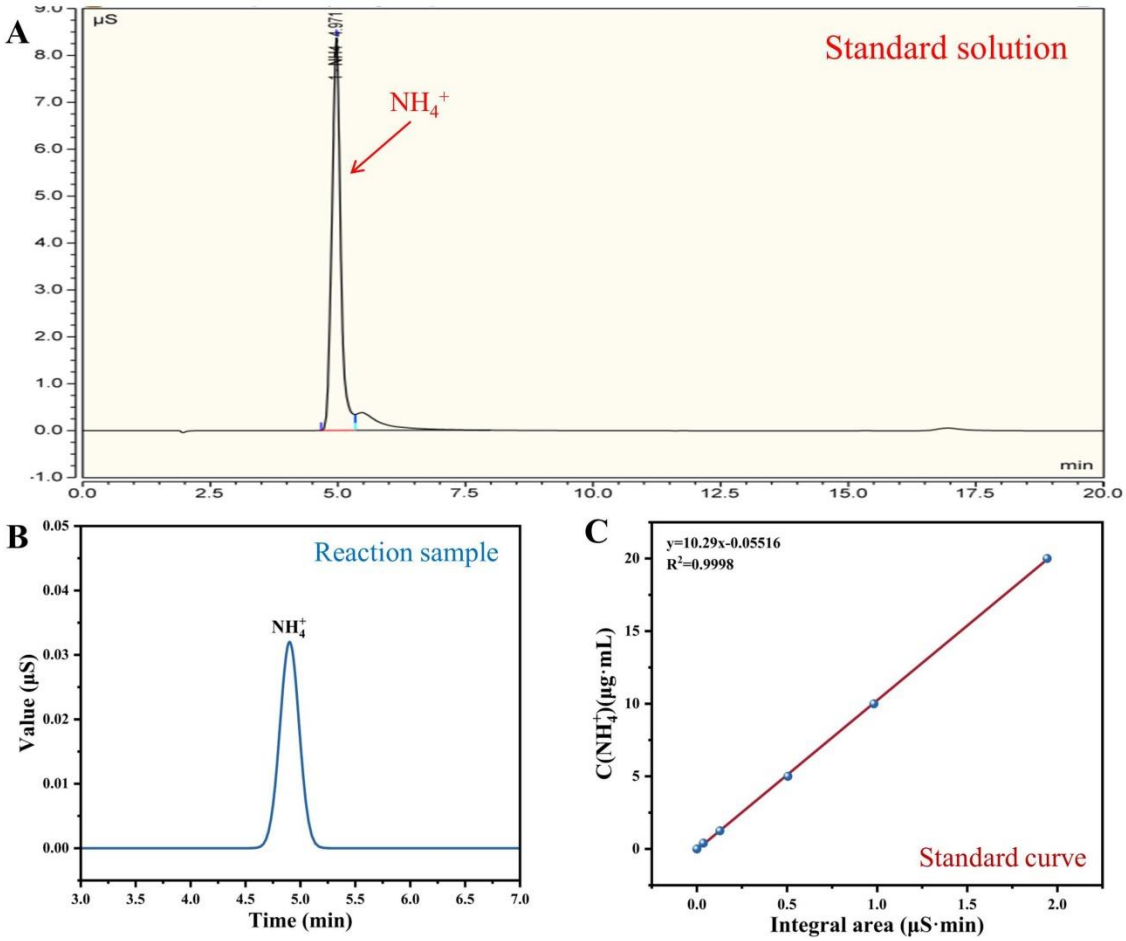

Supplementary Fig.S35 Ion chromatography was used to quantify ammonia product. (A) Ion chromatogram of a sample of 11.95 ug/mL ammonium ion NH_4^+ standard solution. (B) Ion chromatogram of an electrocatalytic reaction sample collected from SiW_{12} solution after reaction 4h. Reaction solution: 0.5g SiW_{12}, 35mL H_2O and 0.05g Ru/TiO_2. (C) Calibration curve for NH_4^+ concentration related to the chromatographic peak area. The ammonia in the sample reaction solution was determined respectively as 1.39 ug/mL by ion chromatography and 1.27 ug/mL by Nessler' reagents.

5. Interaction determination between SiW_{12} and catalyst Ru/TiO_2

From the discussions in main body of this work, the adsorption and desorption kinetic experiments show that the SiW_{12} anions can be adsorbed on Ru/TiO_2 and have strong interactions with the Ru clusters. The element distributions from TEM images further suggest that the element Si has almost the same distribution as the element of Ru (see Fig.4b in main body of this work). Moreover, from the structure of SiW_{12} as shown in Supplementary Fig.S36, we can find that the Si is located in the center of the Keggin-structured SiW_{12} anion. These experimental facts confirm that the adsorbed SiW_{12} anions are distributed on the Ru clusters of Ru/TiO_2.

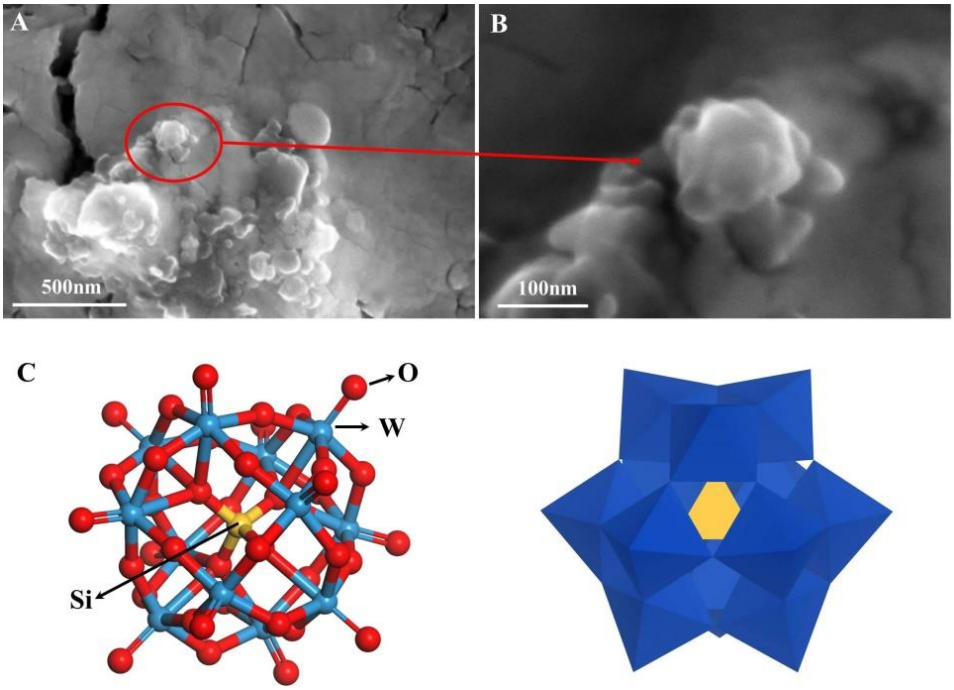

Supplementary Fig.S36 (A) and (B) are SEM images of SiW_{12}; (C) A Keggin-type polyoxometalate SiW_{12} with Keggin-structured $[SiW_{12}]^{4-}$ anion.

In order to further evaluate the interactions of SiW_{12} with Ru, the XPS spectra were used to check what kind of interactions (physical or chemical) between SiW_{12} and Ru. Herein, the XPS spectra of Ru/TiO_2 (Ru 3p and O 1s) and SiW_{12} (W 4f and O 1s) are shown in Supplementary Fig.S37 and the XPS spectra of SiW_{12} adsorbed on Ru/TiO_2, [SiW_{12}/Ru/TiO_2 (Ru 3p, W 4f and O 1s)], can be found in Supplementary Fig.S38. It is found that the bond energy values of Ru 3p (**$3p_{3/2}$: 461.54eV and $3p_{1/2}$: 485.55eV**) and O 1s (**O_t 530.17eV, O_b 531.5eV and O_i 533.2eV**) of SiW_{12}/Ru/TiO_2 are almost same with the bond energy values of Ru 3p (**$3p_{3/2}$ 461.18eV and $3p_{1/2}$ 485.18eV**) of Ru/TiO_2 and O 1s (**O_t 530.7eV, O_b 531.5eV and O_i 532.8eV**) of SiW_{12}, in which O_t is the surface terminal oxygen (W=O), O_b is the bridging oxygen (W-O-W) and O_i is the central oxygen (Si-O-Si). The bond energy values of W 4f of SiW_{12}/Ru/TiO_2 (**$4f_{7/2}$ 35.53eV and $4f_{5/2}$ 37.68eV**) are almost same with the bond energy values of W 4f of SiW_{12} (**$4f_{7/2}$: 35.81eV and $4f_{5/2}$: 37.94eV**). All these results indicate that when SiW_{12} is adsorbed on Ru/TiO_2, no bond energy changes, suggesting that there are no chemical bonds formed between SiW_{12} and Ru/TiO_2. This means there are just strong physical interactions between SiW_{12} and Ru/TiO_2 catalyst. The $[SiW_{12}]^{4-}$ or $[SiW_{12}]^{5-}$ anion is about 1nm in size and have many charges, so that the strong Vander Waals force and electrostatic force play important roles in the physical interactions between SiW_{12} and catalyst.

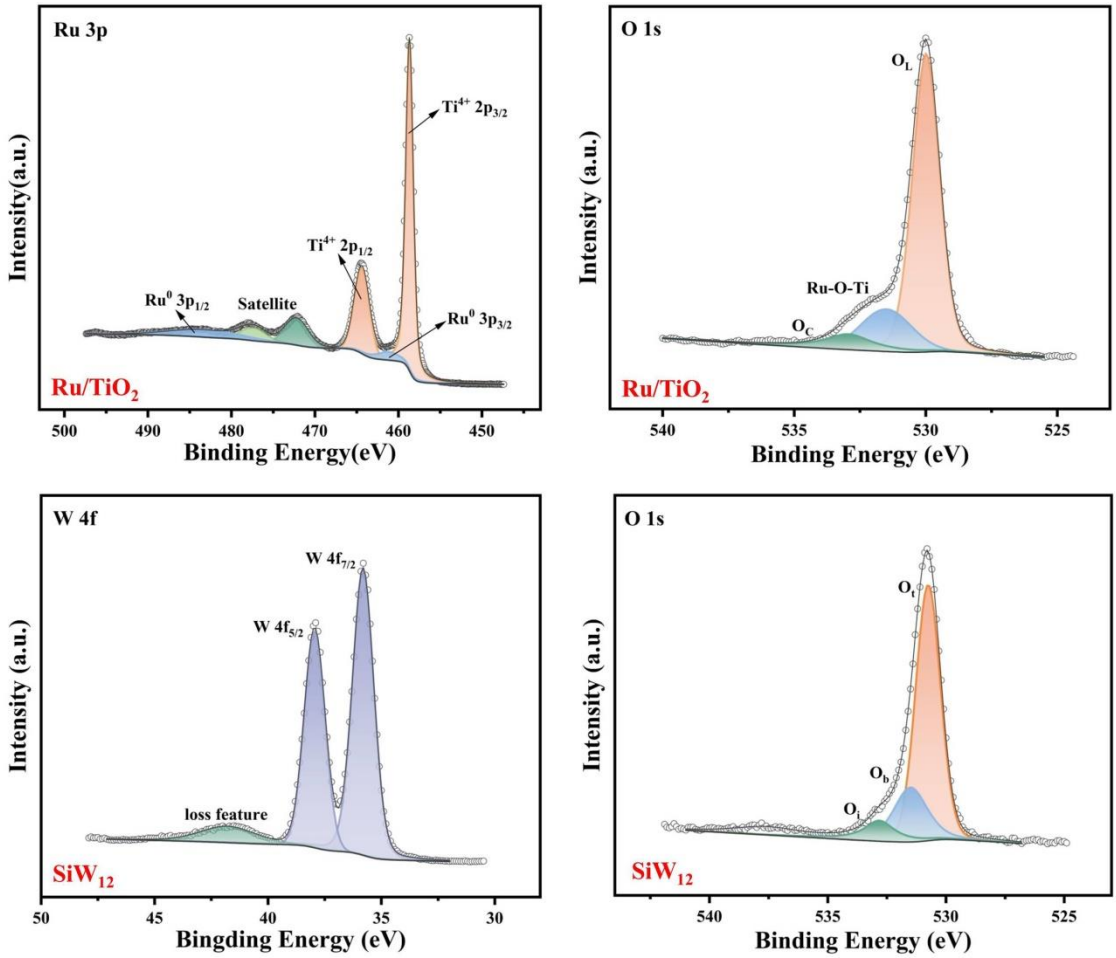

Supplementary Fig.S37 XPS spectra of Ru/TiO_2 (Ru 3p and O 1s) and SiW_{12} (W 4f and O 1s)

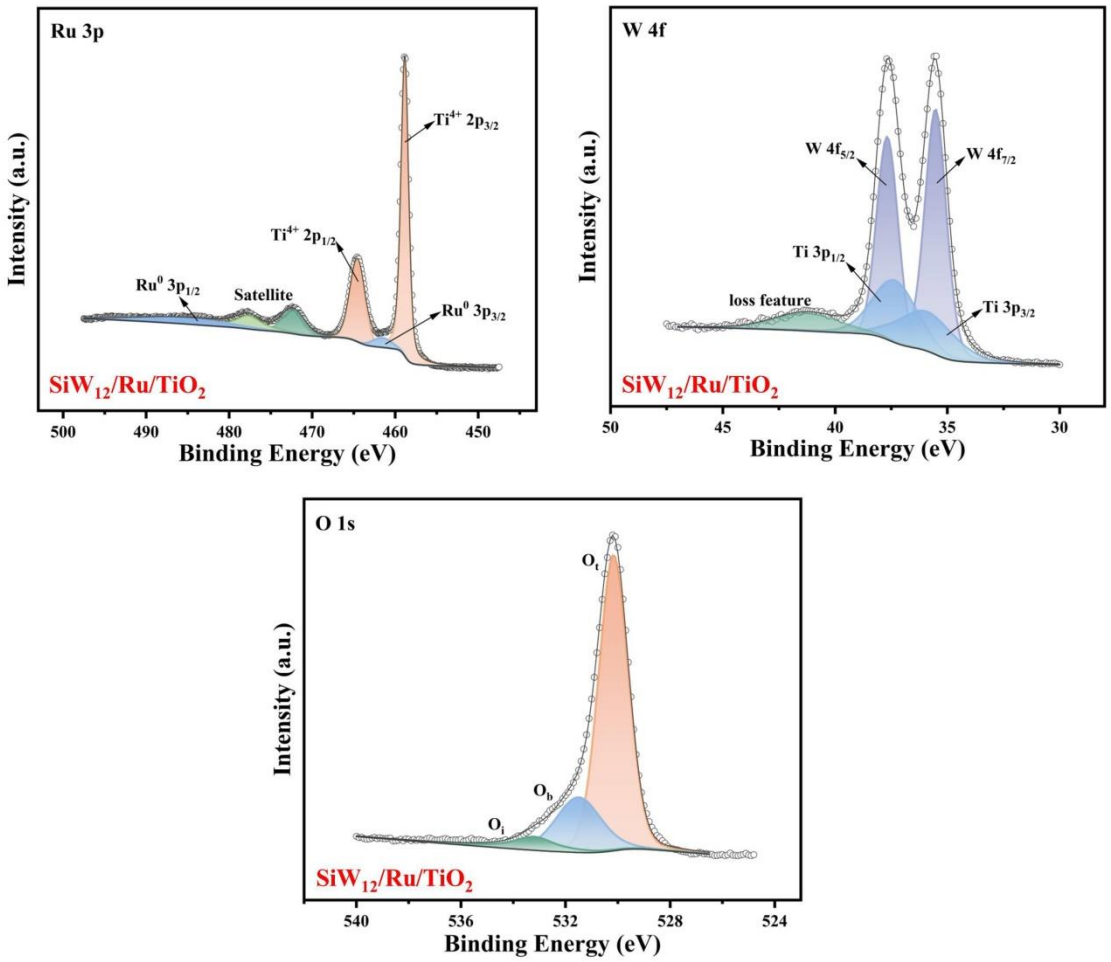

Supplementary Fig.S38 XPS spectra of SiW_{12} adsorbed on Ru/TiO_2 [$SiW_{12}/Ru/TiO_2$ (Ru 3p, W 4f and O 1s)]

6. Comparison of conventional electrolysis with our proposed routes

In conventional electrolysis, the catalysts particles were loaded on the electrode to realize the electrochemical hydrogenation of nitrogen into ammonia as shown in Supplementary Fig.S39. This kind of electrolysis system has some requirements and limits: (1) Catalysts need to be attached on the electrode using some binders, and the binders must be some substances that can conduct electricity. (2) The electrons coming from the electrode need to be transferred to the active sites on catalysts, so that the materials consisting of catalysts also need to conduct electricity. This could results in some limits in using many non-conductive materials that are very efficient to be as catalysts or supports. (3) The space for the catalyst particles is limited in the electrode in which the conductive binders also occupy a certain amount of space, so that the shapes and contact area of catalyst particles are limited as well. (4) The nitrogen N_2 gas needed to overcome the diffusion barriers from the bulk electrolyte to reach at the active sites on catalyst particles loaded on electrode. This could limit the reaction rate of ammonia synthesis.

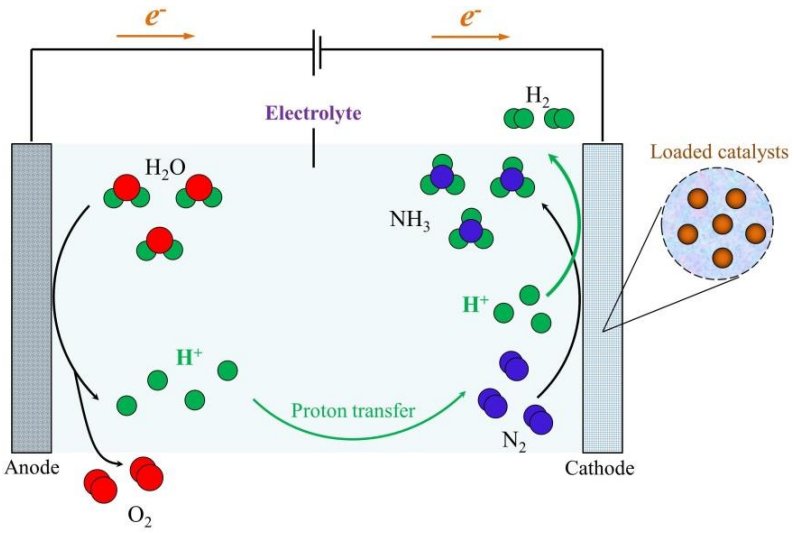

Supplementary Fig.S39 The conventional catalyst-loaded electrochemical system for

nitrogen conversion into ammonia in reported works

However, in our work, a suspended electrolysis system was established to give a novel strategy that uses a combination of a suspended Ru catalyst and water-soluble polyoxometalate SiW_{12} as shown in Supplementary Fig.S40. The SiW_{12} adopted here has multiple functions: First, the electrons can be captured and stored by SiW_{12} which hinders the protons to further react with electrons. Second, SiW_{12} has a low electrical potential which can be easily reduced to negative voltage in water solution, which is essential for reducing target molecules of N_2 with protons. Third, the reduced SiW_{12} can serve as a soluble electron transfer catalyst to transfer the electrons to the Ru catalysts where then the electrons are released to reduce the nitrogen into ammonia.

This suspended dual-catalyst system design could overcome the kinetic diffusion issue and transfer electrons from electrode to suppress hydrogen evolution, so that the electrochemical reaction rate and faradaic efficiency are greatly improved. Because the catalyst particles are not attached on the electrode, the electrons involved in the reactions are delivered by the electron transfer catalyst SiW_{12} rather than direct electric current flow through the catalyst particles. As a result, the required electric conductivity of catalyst particles is no longer limited in this study. This is impossible in conventional electrolysis system which strictly requires the electrons coming from the electrode. This kind of novel design is very different from the traditional ones and has giant significance because there are no limits in the range of catalyst designs and selection of various supports in the electrocatalytic hydrogenation. No matter what kinds of catalysts with different shapes, sizes, geometries, materials and conductive or

non-conductive, all can be used in this electron transfer catalyst enhanced electrolysis system. Even the homogeneous catalysts also can be used in this work, but cannot be used in the conventional ones due to the unique flow characteristics of homogeneous catalysts. In addition, the nitrogen hydrogenation reaction was transferred to occur on the suspended catalysts. This greatly leaves us more opportunities and operations to intensify the nitrogen fixation process, but not affect the electron transfer process on electrode.

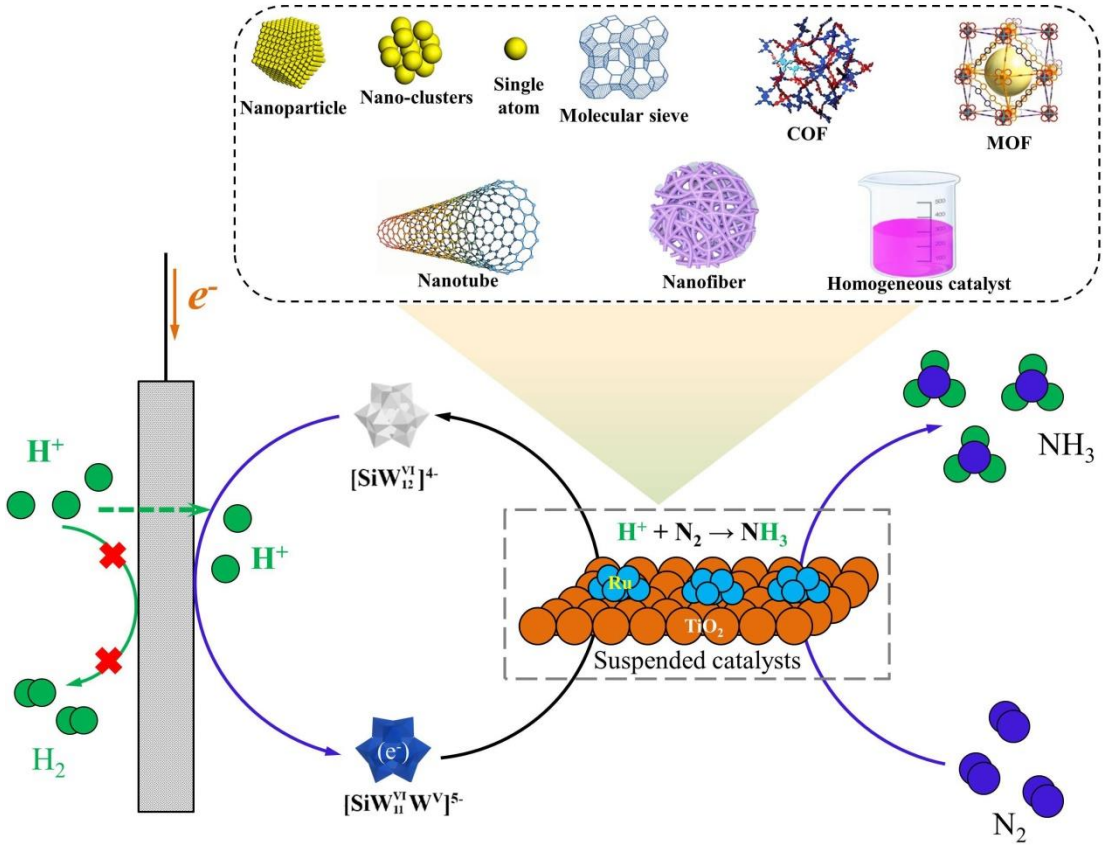

Supplementary Fig.S40 The proposed suspended-catalyst electrochemical system for nitrogen conversion into ammonia in this work

Appendix

1. Comparison of ammonia synthesis at constant current and constant potential

In order to compare, the electrolysis of ammonia synthesis at a constant current density (0.1mA mA/cm^2) and a constant potential (-0.04V vs NHE, 0.1mA mA/cm^2) is also conducted and the results are shown in Supplementary Fig.S41. It can be found that these two methods have similar results as long as the current density keeps same with each other. Therefore, in this work, the electrolysis at constant current density is chosen because it is very convenient to calculate the Faraday efficiency.

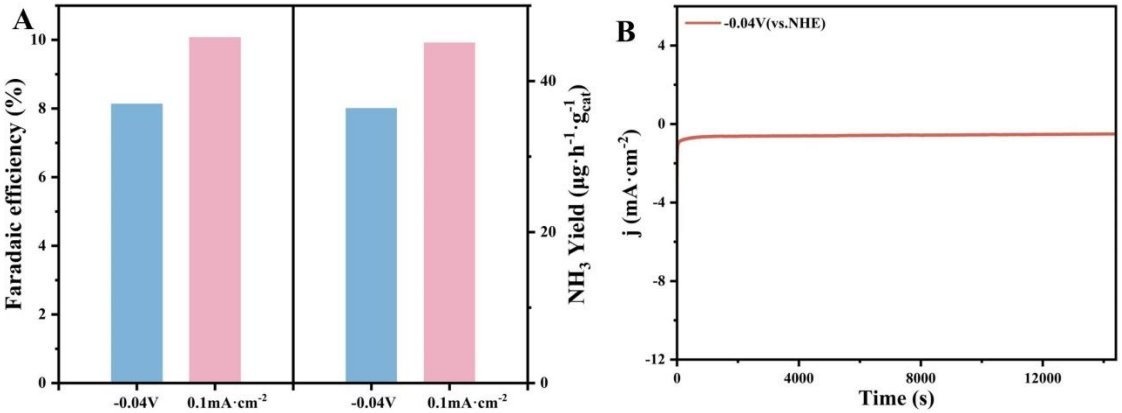

Supplementary Fig.S41 Comparison of electrolysis of ammonia synthesis between constant current (0.1mA/cm^2) and constant potential (-0.04V *vs* NHE, 0.1mA/cm^2).

2. Experimental details and errors summarized in Table.A1

Table.A1 Summarized experimental results of electrocatalytic ammonia synthesis

Experimental conditions	Current density (mA/cm^2)	FE (%)			FE average (%)	Error (%)
		First	Second	Third		
35mL water 5mM SiW_{12} 0.05g Ru/C	100	0.00739	0.00712	0.00796	0.00749	1.34~6.27
	10	0.0942	0.0894	0.102	0.0952	1.05~7.14
	1	0.325	0.375	0.332	0.344	3.49~9.01
	0.1	1.597	1.308	1.349	1.418	4.87~12.6
35mL water 5mM SiW_{12} 0.05g Rh/C	100	——	——	——	——	
	10	——	——	——	——	
	1	——	——	——	——	
	0.1	——	——	——	——	
35mL water 5mM SiW_{12} 0.05g Pd/C	100	0.00129	0.00137	0.00156	0.00142	3.52~9.86
	10	——	——	——	——	
	1	——	——	——	——	
	0.1	——	——	——	——	
35mL water 5mM SiW_{12} 0.05g Pt/C	100	——	——	——	——	
	10	——	——	——	——	
	1	——	——	——	——	
	0.1	——	——	——	——	
35mL water 5mM SiW_{12} 0.05g Ru/TiO_2	100	0.0475	0.0485	0.0531	0.0497	2.41~6.84
	10	0.248	0.286	0.273	0.269	1.49~7.81
	1	1.775	2.056	2.031	1.954	3.94~9.16
	0.1	11.32	9.57	9.32	10.07	4.97~12.4
35mL water H_3PO_4 0.05g Ru/TiO_2	100	0.00857	0.00928	0.0096	0.00915	1.42~6.77
	10	0.0562	0.0645	0.0623	0.0610	2.13~7.87
	1	0.557	0.609	0.532	0.585	4.1~9.06
	0.1	3.74	3.82	3.12	3.56	5.06~12.4
35mL water CF_3SO_3H 0.05g Ru/TiO_2	100	0.0167	0.0181	0.0162	0.0170	1.76~6.47
	10	0.138	0.159	0.144	0.147	2.04~7.48
	1	0.92	1.08	1.051	1.017	3.34~9.54

		0.1	10.43	9.57	9.76	9.92	1.61~5.14
35mL water 5mM SiW_{12} 0.05g TiO_2		100	0.198	0.178	0.185	0.187	1.07~5.89
		10	——	——	——	——	
		1	——	——	——	——	
		0.1	——	——	——	——	
35mL water 5mM SiW_{12} 0.05g Ru/TiO_2	pH=1	100	0.0504	0.0478	0.0512	0.0498	1.2~4.02
	pH=3	100	0.0298	0.0318	0.0323	0.0313	1.6~4.79
	pH=5	100	0.0279	0.0261	0.0285	0.0275	1.45~5.09
	pH=7	100	0.0158	0.0155	0.0146	0.0153	1.31~4.58
	pH=9	100	0.0125	0.0137	0.0134	0.0132	1.52~5.3
3mL alcohols 32mLwater 5mM SiW_{12} 0.05g Ru/TiO_2	Methanol	100	1.093	1.002	1.124	1.073	1.86~6.62
	Ethanol	100	3.507	3.779	3.898	3.728	1.37~5.93
	n-propanol	100	1.564	1.69	1.756	1.67	1.52~6.35
	Isopropanol	100	——	——	——	——	
3mL ethanol 32mLwater 5mM SiW_{12} 0.05g Ru/TiO_2		100	3.507	3.779	3.898	3.728	1.37~5.93
		10	5.073	5.551	5.765	5.463	1.61~7.12
		1	6.081	5.403	6.282	5.922	2.69~8.76
		0.1	38.82	43.77	46.2	42.93	1.96~9.57

*—— means undetected

References

[1] B. Yu, H. Li, J. White, S. Donne, J. Yi, S. Xi, Y. Fu, G. Henkelman, H. Yu, Z. Chen, T. Ma, Tuning the Catalytic Preference of Ruthenium Catalysts for Nitrogen Reduction by Atomic Dispersion, Adv. Funct. Mater. 30 (2020) 1905665. https://doi.org/https://doi.org/10.1002/adfm.201905665.

[2] H. Tao, C. Choi, L.-X. Ding, Z. Jiang, Z. Han, M. Jia, Q. Fan, Y. Gao, H. Wang, A.W. Robertson, S. Hong, Y. Jung, S. Liu, Z. Sun, Nitrogen Fixation by Ru Single-Atom Electrocatalytic Reduction, Chem. 5 (2019) 204–214. https://doi.org/https://doi.org/10.1016/j.chempr.2018.10.007.

[3] Z. Geng, Y. Liu, X. Kong, P. Li, K. Li, Z. Liu, J. Du, M. Shu, R. Si, J. Zeng, Achieving a Record-High Yield Rate of 120.9 for N2 Electrochemical Reduction over Ru Single-Atom Catalysts, Adv. Mater. 30 (2018) 1803498. https://doi.org/https://doi.org/10.1002/adma.201803498.

[4] W. Peng, M. Luo, X. Xu, K. Jiang, M. Peng, D. Chen, T.-S. Chan, Y. Tan, Spontaneous Atomic Ruthenium Doping in Mo2CTX MXene Defects Enhances Electrocatalytic Activity for the Nitrogen Reduction Reaction, Adv. Energy Mater. 10 (2020) 2001364. https://doi.org/https://doi.org/10.1002/aenm.202001364.

[5] R. Zhao, C. Liu, X. Zhang, X. Zhu, P. Wei, L. Ji, Y. Guo, S. Gao, Y. Luo, Z. Wang, X. Sun, An ultrasmall Ru2P nanoparticles–reduced graphene oxide hybrid: an efficient electrocatalyst for NH3 synthesis under ambient conditions, J. Mater. Chem. A. 8 (2020) 77–81. https://doi.org/10.1039/C9TA10346E.

[6] X. Wang, W. Wang, M. Qiao, G. Wu, W. Chen, T. Yuan, Q. Xu, M. Chen, Y. Zhang, X. Wang,

J. Wang, J. Ge, X. Hong, Y. Li, Y. Wu, Y. Li, Atomically dispersed Au1 catalyst towards efficient electrochemical synthesis of ammonia, Sci. Bull. 63 (2018) 1246–1253. https://doi.org/https://doi.org/10.1016/j.scib.2018.07.005.

[7] C. He, Z.-Y. Wu, L. Zhao, M. Ming, Y. Zhang, Y. Yi, J.-S. Hu, Identification of FeN4 as an Efficient Active Site for Electrochemical N2 Reduction, ACS Catal. 9 (2019) 7311–7317. https://doi.org/10.1021/acscatal.9b00959.

[8] Y. Wang, X. Cui, J. Zhao, G. Jia, L. Gu, Q. Zhang, L. Meng, Z. Shi, L. Zheng, C. Wang, Z. Zhang, W. Zheng, Rational Design of Fe–N/C Hybrid for Enhanced Nitrogen Reduction Electrocatalysis under Ambient Conditions in Aqueous Solution, ACS Catal. 9 (2019) 336–344. https://doi.org/10.1021/acscatal.8b03802.

[9] M. Wang, S. Liu, T. Qian, J. Liu, J. Zhou, H. Ji, J. Xiong, J. Zhong, C. Yan, Over 56.55% Faradaic efficiency of ambient ammonia synthesis enabled by positively shifting the reaction potential, Nat. Commun. 10 (2019) 341. https://doi.org/10.1038/s41467-018-08120-x.

[10] S.-J. Li, D. Bao, M.-M. Shi, B.-R. Wulan, J.-M. Yan, Q. Jiang, Amorphizing of Au Nanoparticles by CeOx–RGO Hybrid Support towards Highly Efficient Electrocatalyst for N2 Reduction under Ambient Conditions, Adv. Mater. 29 (2017) 1700001. https://doi.org/https://doi.org/10.1002/adma.201700001.

[11] M.-M. Shi, D. Bao, B.-R. Wulan, Y.-H. Li, Y.-F. Zhang, J.-M. Yan, Q. Jiang, Au Sub-Nanoclusters on TiO2 toward Highly Efficient and Selective Electrocatalyst for N2 Conversion to NH3 at Ambient Conditions, Adv. Mater. 29 (2017) 1606550. https://doi.org/https://doi.org/10.1002/adma.201606550.

[12] G.-F. Chen, X. Cao, S. Wu, X. Zeng, L.-X. Ding, M. Zhu, H. Wang, Ammonia

Electrosynthesis with High Selectivity under Ambient Conditions via a Li+ Incorporation Strategy, J. Am. Chem. Soc. 139 (2017) 9771–9774. https://doi.org/10.1021/jacs.7b04393.

[13] Y. Liu, Y. Su, X. Quan, X. Fan, S. Chen, H. Yu, H. Zhao, Y. Zhang, J. Zhao, Facile Ammonia Synthesis from Electrocatalytic N2 Reduction under Ambient Conditions on N-Doped Porous Carbon, ACS Catal. 8 (2018) 1186–1191. https://doi.org/10.1021/acscatal.7b02165.

[14] E. Vasileiou, V. Kyriakou, I. Garagounis, A. Vourros, M. Stoukides, Ammonia synthesis at atmospheric pressure in a BaCe0.2Zr0.7Y0.1O2.9 solid electrolyte cell, Solid State Ionics. 275 (2015) 110–116. https://doi.org/https://doi.org/10.1016/j.ssi.2015.01.002.

[15] F. Zhang, Q. Yang, B. Pan, R. Xu, H. Wang, G. Ma, Proton conduction in La0.9Sr0.1Ga0.8Mg0.2O3−α ceramic prepared via microemulsion method and its application in ammonia synthesis at atmospheric pressure, Mater. Lett. 61 (2007) 4144–4148. https://doi.org/https://doi.org/10.1016/j.matlet.2007.01.060.

[16] D.S. Yun, J.H. Joo, J.H. Yu, H.C. Yoon, J.-N. Kim, C.-Y. Yoo, Electrochemical ammonia synthesis from steam and nitrogen using proton conducting yttrium doped barium zirconate electrolyte with silver, platinum, and lanthanum strontium cobalt ferrite electrocatalyst, J. Power Sources. 284 (2015) 245–251. https://doi.org/https://doi.org/10.1016/j.jpowsour.2015.03.002.

[17] J. Otomo, N. Noda, F. Kosaka, Electrochemical Synthesis of Ammonia with Proton Conducting Solid Electrolyte Fuel Cells at Intermediate Temperatures, ECS Trans. 68 (2015) 2663. https://doi.org/10.1149/06801.2663ecst.

[18] Y. Guo, B. Liu, Q. Yang, C. Chen, W. Wang, G. Ma, Preparation via microemulsion method and proton conduction at intermediate-temperature of BaCe1−xYxO3−α, Electrochem.

Commun. 11 (2009) 153–156. https://doi.org/https://doi.org/10.1016/j.elecom.2008.10.038.

[19] I.A. Amar, C.T.G. Petit, L. Zhang, R. Lan, P.J. Skabara, S. Tao, Electrochemical synthesis of ammonia based on doped-ceria-carbonate composite electrolyte and perovskite cathode, Solid State Ionics. 201 (2011) 94–100. https://doi.org/https://doi.org/10.1016/j.ssi.2011.08.003.

[20] I.A. Amar, R. Lan, C.T.G. Petit, S. Tao, Electrochemical Synthesis of Ammonia Based on Co3Mo3N Catalyst and LiAlO2–(Li,Na,K)2CO3 Composite Electrolyte, Electrocatalysis. 6 (2015) 286–294. https://doi.org/10.1007/s12678-014-0242-x.

[21] I.A. Amar, R. Lan, C.T.G. Petit, V. Arrighi, S. Tao, Electrochemical synthesis of ammonia based on a carbonate-oxide composite electrolyte, Solid State Ionics. 182 (2011) 133–138. https://doi.org/https://doi.org/10.1016/j.ssi.2010.11.009.

[22] I.A. Amar, R. Lan, S. Tao, Electrochemical Synthesis of Ammonia Directly from Wet N2 Using La0.6Sr0.4Fe0.8Cu0.2O3-δ-Ce0.8Gd0.18Ca0.02O2-δ Composite Catalyst, J. Electrochem. Soc. 161 (2014) H350. https://doi.org/10.1149/2.021406jes.

[23] T. Murakami, T. Nohira, Y. Araki, T. Goto, R. Hagiwara, Y.H. Ogata, Electrolytic Synthesis of Ammonia from Water and Nitrogen under Atmospheric Pressure Using a Boron-Doped Diamond Electrode as a Nonconsumable Anode, Electrochem. Solid-State Lett. 10 (2007) E4. https://doi.org/10.1149/1.2437674.

[24] T. Murakami, T. Nohira, T. Goto, Y.H. Ogata, Y. Ito, Electrolytic ammonia synthesis from water and nitrogen gas in molten salt under atmospheric pressure, Electrochim. Acta. 50 (2005) 5423–5426. https://doi.org/https://doi.org/10.1016/j.electacta.2005.03.023.

[25] S. Licht, B. Cui, B. Wang, F.-F. Li, J. Lau, S. Liu, RETRACTED: Ammonia synthesis by N2 and steam electrolysis in molten hydroxide suspensions of nanoscale Fe2O3, Science (80-.).

345 (2014) 637–640. https://doi.org/10.1126/science.1254234.

[26] F.-F. Li, S. Licht, Advances in Understanding the Mechanism and Improved Stability of the Synthesis of Ammonia from Air and Water in Hydroxide Suspensions of Nanoscale Fe2O3, Inorg. Chem. 53 (2014) 10042–10044. https://doi.org/10.1021/ic5020048.

[27] V. Kordali, G. Kyriacou, C. Lambrou, Electrochemical synthesis of ammonia at atmospheric pressure and low temperature in a solid polymer electrolyte cell, Chem. Commun. (2000) 1673–1674. https://doi.org/10.1039/B004885M.

[28] R. Lan, S. Tao, Electrochemical synthesis of ammonia directly from air and water using a Li+/H+/NH4+ mixed conducting electrolyte, RSC Adv. 3 (2013) 18016–18021. https://doi.org/10.1039/C3RA43432J.

[29] M. Kitano, S. Kanbara, Y. Inoue, N. Kuganathan, P. V Sushko, T. Yokoyama, M. Hara, H. Hosono, Electride support boosts nitrogen dissociation over ruthenium catalyst and shifts the bottleneck in ammonia synthesis, Nat. Commun. 6 (2015) 6731–9. https://doi.org/10.1038/ncomms7731.

[30] M. Kitano, Y. Inoue, Y. Yamazaki, F. Hayashi, S. Kanbara, S. Matsuishi, T. Yokoyama, S.-W. Kim, M. Hara, H. Hosono, Ammonia synthesis using a stable electride as an electron donor and reversible hydrogen store, Nat. Chem. 4 (2012) 934–940. https://doi.org/10.1038/nchem.1476.

[31] Y. Inoue, M. Kitano, S.-W. Kim, T. Yokoyama, M. Hara, H. Hosono, Highly dispersed Ru on electride [Ca24Al28O64]4+(e–)4 as a catalyst for ammonia synthesis, ACS Catal. 4 (2014) 674–680. https://doi.org/10.1021/cs401044a.

[32] M. Kitano, Y. Inoue, H. Ishikawa, K. Yamagata, T. Nakao, T. Tada, S. Matsuishi, T. Yokoyama, M. Hara, H. Hosono, Essential role of hydride ion in ruthenium-based ammonia

synthesis catalysts, Chem. Sci. 7 (2016) 4036–4043. https://doi.org/10.1039/C6SC00767H.

[33] M. Hattori, T. Mori, T. Arai, Y. Inoue, M. Sasase, T. Tada, M. Kitano, T. Yokoyama, M. Hara, H. Hosono, Enhanced catalytic ammonia synthesis with transformed BaO, ACS Catal. 8 (2018) 10977–10984. https://doi.org/10.1021/acscatal.8b02839.

[34] Y. Lu, J. Li, T. Tada, Y. Toda, S. Ueda, T. Yokoyama, M. Kitano, H. Hosono, Water durable electride Y5Si3: electronic structure and catalytic activity for ammonia synthesis, J. Am. Chem. Soc. 138 (2016) 3970–3973. https://doi.org/10.1021/jacs.6b00124.

[35] J. Wu, Y. Gong, T. Inoshita, D.C. Fredrickson, J. Wang, Y. Lu, M. Kitano, H. Hosono, Tiered electron anions in multiple voids of LaScSi and their applications to ammonia synthesis, Adv. Mater. 29 (2017) 1700924. https://doi.org/https://doi.org/10.1002/adma.201700924.

[36] Y. Inoue, M. Kitano, M. Tokunari, T. Taniguchi, K. Ooya, H. Abe, Y. Niwa, M. Sasase, M. Hara, H. Hosono, Direct activation of cobalt catalyst by 12CaO·7Al2O3 electride for ammonia synthesis, ACS Catal. 9 (2019) 1670–1679. https://doi.org/10.1021/acscatal.8b03650.

[37] R. Kojima, K. Aika, Cobalt molybdenum bimetallic nitride catalysts for ammonia synthesis: Part 2. Kinetic study, Appl. Catal. A Gen. 218 (2001) 121–128. https://doi.org/https://doi.org/10.1016/S0926-860X(01)00626-3.

[38] M. Hattori, S. Iijima, T. Nakao, H. Hosono, M. Hara, Solid solution for catalytic ammonia synthesis from nitrogen and hydrogen gases at 50 °C, Nat. Commun. 11 (2020) 2001. https://doi.org/10.1038/s41467-020-15868-8.

[39] T. Bécue, R.J. Davis, J.M. Garces, Effect of cationic promoters on the kinetics of ammonia synthesis catalyzed by ruthenium supported on zeolite X, J. Catal. 179 (1998) 129–137. https://doi.org/https://doi.org/10.1006/jcat.1998.2212.

[40] S. Hagen, R. Barfod, R. Fehrmann, C.J.H. Jacobsen, H.T. Teunissen, I. Chorkendorff, Ammonia synthesis with barium-promoted iron–cobalt alloys supported on carbon, J. Catal. 214 (2003) 327–335. https://doi.org/https://doi.org/10.1016/S0021-9517(02)00182-3.

[41] P. Wang, F. Chang, W. Gao, J. Guo, G. Wu, T. He, P. Chen, Breaking scaling relations to achieve low-temperature ammonia synthesis through LiH-mediated nitrogen transfer and hydrogenation, Nat. Chem. 9 (2017) 64–70. https://doi.org/10.1038/nchem.2595.

[42] B. Keita, L. Nadjo, New aspects of the electrochemistry of heteropolyacids: Part II. Coupled electron and proton transfers in the reduction of silicoungstic species, J. Electroanal. Chem. Interfacial Electrochem. 217 (1987) 287–304. https://doi.org/https://doi.org/10.1016/0022-0728(87)80225-5.

[43] Y. Guo, R. Zhang, S. Zhang, Y. Zhao, Q. Yang, Z. Huang, B. Dong, C. Zhi, Pd doping-weakened intermediate adsorption to promote electrocatalytic nitrate reduction on TiO2 nanoarrays for ammonia production and energy supply with zinc–nitrate batteries, Energy Environ. Sci. 14 (2021) 3938–3944. https://doi.org/10.1039/D1EE00806D.

[44] X. Zeng, Y. Bai, S.M. Choi, L. Tong, R.M. Aleisa, Z. Li, X. Liu, R. Yu, N. V Myung, Y. Yin, Mesoporous TiO2 nanospheres loaded with highly dispersed Pd nanoparticles for pH-universal hydrogen evolution reaction, Mater. Today Nano. 6 (2019) 100038. https://doi.org/https://doi.org/10.1016/j.mtnano.2019.100038.

[45] H. Ye, Q. Wang, M. Catalano, N. Lu, J. Vermeylen, M.J. Kim, Y. Liu, Y. Sun, X. Xia, Ru Nanoframes with an fcc Structure and Enhanced Catalytic Properties, Nano Lett. 16 (2016) 2812–2817. https://doi.org/10.1021/acs.nanolett.6b00607.

[46] N. Kruse, S. Chenakin, XPS characterization of Au/TiO2 catalysts: Binding energy assessment

and irradiation effects, Appl. Catal. A Gen. 391 (2011) 367–376. https://doi.org/https://doi.org/10.1016/j.apcata.2010.05.039.

[47] R. Castillo, B. Koch, P. Ruiz, B. Delmon, Influence of the Amount of Titania on the Texture and Structure of Titania Supported on Silica, J. Catal. 161 (1996) 524–529. https://doi.org/https://doi.org/10.1006/jcat.1996.0214.

[48] M. Wang, G. Li, S. Wang, X. Liu, A. Wang, H. Cao, C. Zhang, Catalytic oxidation of propane over nanorod-like TiO2 supported Ru catalysts: Structure-activity dependence and mechanistic insights, Chem. Eng. J. 481 (2024) 148344. https://doi.org/https://doi.org/10.1016/j.cej.2023.148344.

[49] L. Jing, G. Jie, W. Yu, H. Ren, X. Cui, X. Chen, L. Jiang, A unique sandwich-structured Ru-TiO/TiO2@NC as an efficient bi-functional catalyst for hydrogen oxidation and hydrogen evolution reactions, Chem. Eng. J. 472 (2023) 145009. https://doi.org/https://doi.org/10.1016/j.cej.2023.145009.

[50] R. Bavand, A. Yelon, E. Sacher, X-ray photoelectron spectroscopic and morphologic studies of Ru nanoparticles deposited onto highly oriented pyrolytic graphite, Appl. Surf. Sci. 355 (2015) 279–289. https://doi.org/https://doi.org/10.1016/j.apsusc.2015.06.202.

[51] W. Cai, Y.-F. Jiang, J. Zhang, H. Yang, J. Zhang, C.-Q. Xu, W. Liu, J. Li, B. Liu, Ruthenium/titanium oxide interface promoted electrochemical nitrogen reduction reaction, Chem Catal. 2 (2022) 1764–1774. https://doi.org/10.1016/j.checat.2022.05.009.